Supporting Information
for

Anti-myeloma pro-apoptotic Pt(II) diiodido complexes

Lukáš Masaryk,[a,1] Denisa Weiser Drozdková,[b,c,1] Karolina Słoczyńska,[d] Ján Moncol',[e] David Milde,[f] Radka Křikavová,[a] Justyna Popiół,[d] Elżbieta Pękala,[d] Katarína Ondrušková,[b] Ivan Nemec,[a,h,*] Kateřina Smešný Trtková,[b,c,g,**] and Pavel Štarha[a,***]

[a] *Department of Inorganic Chemistry, Faculty of Science, Palacký University Olomouc, 17. listopadu 12, 77146 Olomouc, Czech Republic*
[b] *Department of Clinical and Molecular Pathology, Faculty of Medicine and Dentistry, Palacký University Olomouc, Hněvotínská 3, 77515 Olomouc, Czech Republic*
[c] *Institute of Molecular and Clinical Pathology and Medical Genetics, Faculty of Medicine, University of Ostrava, Syllabova 19, 703 00 Ostrava – Vítkovice, Czech Republic*
[d] *Department of Pharmaceutical Biochemistry, Faculty of Pharmacy, Jagiellonian University Medical College, Medyczna 9, 30-688 Kraków, Poland*
[e] *Department of Inorganic Chemistry, Faculty of Chemical and Food Technology, Slovak University of Technology in Bratislava, 81237 Bratislava, Slovakia*
[f] *Department of Analytical Chemistry, Faculty of Science, Palacký University Olomouc, 17. listopadu 12, 77146 Olomouc, Czech Republic*
[g] *Institute of Molecular and Translational Medicine, Faculty of Medicine and Dentistry, Palacký University Olomouc, Hněvotínská 5, 77515 Olomouc, Czech Republic*
[h] *Central European Institute of Technology, Brno University of Technology, Purkyňova 123, 61200 Brno, Czech Republic*

[1] These authors contributed equally to this work
Corresponding authors: Pavel Štarha (***), pavel.starha@upol.cz; Kateřina Smešný Trtková (**), katerina.smesny@upol.cz; Ivan Nemec (*), ivan.nemec@upol.cz

Table of Contents

Experimental section

Chemicals

Potassium tetrachloridoplatinate(II) ($K_2[PtCl_4]$) was purchased from Precious Metals Online, while 1-methyl-1*H*-imidazole (L^1), 1-benzyl-1*H*-imidazole (L^2), 1-benzyl-2-methyl-1*H*-imidazole (L^3), 1-phenyl-1*H*-imidazole (L^4), 1-(4-methoxyphenyl)-1*H*-imidazole (L^5), 1-(4-fluorophenyl)-1*H*-imidazole (L^6), 1-(4-chlorophenyl)-1*H*-imidazole (L^7), potassium iodide, cisplatin, GSH, guanosine 5′-monophosphate disodium salt hydrate, PBS, solvents (methanol, diethyl ether, ethanol, DMF, DMSO and *n*-octanol) and deuterated solvents for NMR experiments (DMF-d_7 and D_2O) were supplied by VWR International (Stříbrná Skalice, Czech Republic), Sigma-Aldrich (Prague, Czech Republic), Lach-Ner (Neratovice, Czech Republic) and Litolab (Chudobín, Czech Republic). Fetal Bovine Serum (FBS; Gibco, Waltham, MA, USA), streptomycin/penicillin mixture (Sigma-Aldrich, Darmstadt, Germany), L-glutamine (Sigma-Aldrich, Darmstadt, Germany), sodium pyruvate (Thermo Fisher Scientific, Waltham, MA, USA), ApoScreenR Annexin-V, CellEvent™ Caspase-3/7 Green, HEPES, propidium iodide (PI), 4',6-diamidine-2'-phenylindole dihydrochloride (DAPI), 7-aminoactinomycin D (Sigma-Aldrich (St. Louis, MO, USA) were purchased from the given commercial sources.

Synthesis

The solution of $K_2[PtCl_4]$ (0.1 mmol) in 1 mL of deionized water was heated to 50 °C and 5 molar equiv. of potassium iodide was added. The reaction mixture was let to cool down to ambient temperature with stirring (10 min), providing a solution of $K_2[PtI_4]$. After that, imidazole derivatives (L^n; 0.2 mmol) dissolved in 1 mL of MeOH were added dropwise to $K_2[PtI_4]$. The obtained brownish suspension was stirred for 24 h at ambient temperature, then the obtained yellow-brown solid was collected by filtration and washed with water (2 × 0.5 mL), methanol (2 × 0.5 mL) and diethyl ether (2 × 1 mL). The solid products were dried in a desiccator under reduced pressure (overnight).

cis-$[PtI_2(L^1)_2]$ (**1**): Yellow solid. Yield 90%. Anal. Calcd. for $C_8H_{12}I_2N_4Pt$: C, 15.69; H, 1.97; N, 9.14%; found: C, 15.48; H, 2.07; N, 8.94%. ^{1}H NMR (400 MHz, DMF-d_7, 298 K, ppm): δ 8.23 (s, 1H, C2-H), 7.35 (s, 1H, C5-H), 7.09 (s, 1H, C4-H), 3.81 (s, 3H, C6-H). ^{13}C NMR (101 MHz, DMF-d_7, 298 K, ppm): δ 140.0 (C2), 129.1 (C4), 121.7 (C5), 34.2 (C6). ^{195}Pt NMR (86 MHz, DMF-d_7, 298 K, ppm): δ -3108. ESI+ MS (MeOH, *m/z*): 652.0 (calc. 652.2; 100%; $\{[PtI_2(L^1)_2]+H\}^+$). IR (ATR, ν, cm^{-1}): 353s, 615w, 649w, 757w, 809w, 1093m, 1234w, 1283w, 1420w, 1520m, 1616w, 1721w, 3106m.

cis-$[PtI_2(L^2)_2]\cdot H_2O$ (**2**): Yellow solid. Yield 92%. Anal. Calcd. for $C_{20}H_{20}I_2N_4Pt\cdot H_2O$: C, 30.67; H, 2.83; N, 7.15%; found: C, 30.62; H, 3.02; N, 6.90%. ^{1}H NMR (400 MHz, DMF-d_7, 298 K, ppm): δ 8.45 (s, 1H, C2-H), 7.43–7.27 (m, 6H, C5-H, C8-12-H), 7.10 (s, 1H, C4-H), 5.40 (s,

2H, C6-H). ^{13}C NMR (101 MHz, DMF-d_7, 298 K, ppm): δ 139.8 (C2), 136.9 (C7), 129.5 (C4), 129.1 (C9, C11), 128.4 (C10), 128.0 (C8,12), 120.7 (C5), 51.2 (C6). ^{195}Pt NMR (86 MHz, DMF-d_7, 298 K, ppm): δ -3119. ESI+ MS (MeOH, *m/z*): 788.0 (calc. 788.3; 100%; {[$PtI_2(L^2)_2$] + Na^+}$^+$). IR (ATR, ν, cm^{-1}): 340s, 442w, 569w, 628w, 674w, 700w, 743s, 762s, 1020w, 1161m, 1199w, 1253w, 1421m, 1439w, 1501s, 1550w, 1594w, 3097m, 3121w.

cis-[$PtI_2(L^3)_2$] (**3**): Brown solid. Yield 85%. Anal. Calcd. for $C_{22}H_{24}I_2N_4Pt$: C, 33.31; H, 3.05; N, 7.06%; found: C, 33.56; H, 3.32; N, 7.41%. ^{1}H NMR (400 MHz, DMF-d_7, 298 K, ppm): δ 7.37–7.28 (m, 4H, C5-H, C9-11-H), 7.24 (s, 1H, C4-H), 7.08–7.03 (m, 2H, C8-H, C12-H), 5.32 (s, 2H, C6-H), 2.68 (s, 3H, C13-H). ^{13}C NMR (101 MHz, DMF-d_7, 298 K, ppm): δ 145.4 (C2), 136.2 (C7), 128.7 (C9,11), 127.7 (C10), 127.5 (C4), 126.6 (C8,12), 121.2 (C5), 49.95 (C6), 13.6 (C13). ^{195}Pt NMR (86 MHz, DMF-d_7, 298 K, ppm): δ -3185. ESI+ MS (MeOH, *m/z*): 666.1 (calc. 666.1; 45%; [$PtI(L^3)_2]^+$), 832.1 (calc. 831.9; 40%; {[$PtI_2(L^3)_2$] + K^+}$^+$). IR (ATR, ν, cm^{-1}): 345s, 447w, 575w, 632w, 670w, 695m, 723s, 751s, 945w, 1160m, 1278m, 1352w, 1430m, 1444m, 1497s, 1549w, 1602w, 3026w, 3114m, 3136w, 3444w.

cis-[$PtI_2(L^4)_2$]·H_2O (**4**): Yellow solid. Yield 89%. Anal. Calcd. for $C_{18}H_{16}I_2N_4Pt·H_2O$: C, 28.63; H, 2.40; N, 7.42%; found: C, 28.33; H, 2.59; N, 7.44%. ^{1}H NMR (400 MHz, DMF-d_7, 298 K, ppm): δ 9.02 (s, 1H, C2-H), 8.02 (s, 1H, C5-H), 7.77 (d, *J* = 8.0 Hz, 2H, C7-H, C11-H), 7.58 (t, *J* = 8.0 Hz, 2H, C8-H, C10-H), 7.51–7.40 (m, 2H, C4-H, C9-H). ^{13}C NMR (101 MHz, DMF-d_7, 298 K, ppm): δ 137.9 (C2), 136.3 (C6), 130.7 (C4), 130.3 (C8,10), 128.6 (C9), 121.2 (C7,11), 119.3 (C5). ^{195}Pt NMR (86 MHz, DMF-d_7, 298 K, ppm): δ -3114. ESI+ MS (MeOH, *m/z*): 482.3 (calc. 482.4; 5%; {[$Pt(L^4)_2$] - H^+}$^+$), 610.1 (calc. 610.3; 66%; [$PtI(L^4)_2]^+$), 664.3 (calc. 664.4; 100 %; {[$PtI(L^4)_2$] + $3H_2O$}$^+$), 755.1 (calc.755.3; 100 %; {[$PtI_2(L^4)_2$] + NH_4^+}$^+$), 775.9 (calc. 776.3; 50 %; {[$PtI_2(L^4)_2$] + K^+}$^+$). IR (ATR, ν, cm^{-1}): 396w, 455w, 516w, 644w, 685m, 731m, 747s, 812w, 904w, 963w, 1061m, 1109w, 1132w, 1181w, 1244w, 1307m, 1457w, 1514s, 3045w, 3120m, 3142w.

cis-[$PtI_2(L^5)_2$]·$2H_2O$ (**5**): Yellow solid. Yield 85%. Anal. Calcd. for $C_{20}H_{20}I_2N_4O_2Pt·2H_2O$: C, 30.13; H, 2.53; N, 7.03%; found: C, 30.46; H, 2.61; N, 7.11%. ^{1}H NMR (400 MHz, DMF-d_7, 298 K, ppm): δ 8.83 (s, 1H, C2-H), 7.90 (s, 1H, C5-H), 7.70–7.64 (m, 2H, C7-H, C11-H), 7.36 (s, 1H, C4-H), 7.16–7.09 (m, 2H, C8-H, C10-H), 3.86 (s, 3H, C13-H). ^{13}C NMR (101 MHz, DMF-d_7, 298 K, ppm): δ 159.7 (C9), 137.8 (C2), 130.3 (C4), 129.6 (C6), 122.9 (C7,11), 119.6 (C5), 115.2 (C8,10), 55.6 (C13). ^{195}Pt NMR (86 MHz, DMF-d_7, 298 K, ppm): δ -3150. ESI+ MS (MeOH, *m/z*): 670.2 (calc. 670.4; 35%; [$PtI(L^5)_2]^+$), 753.1 (calc. 753.5; 90%; {[$PtI_2(L^5)_2$] + 2MeOH + H_2O + H^+}$^+$), 820.0 (calc. 820.3; 100 %; {[$PtI_2(L^5)_2$] + Na^+}$^+$). IR (ATR, ν, cm^{-1}): 526w, 614w, 645w, 724w, 797w, 823m, 864w, 1024m, 1061m, 1133w, 1181w, 1252s, 1304w, 1361w, 1458w, 1518vs, 2836w, 2955w, 3118m.

cis-[$PtI_2(L^6)_2$] (**6**): Brown solid. Yield 91%. Anal. Calcd. for $C_{18}H_{14}I_2F_2N_4Pt$: C, 27.96; H, 1.82; N, 7.25 %; found: C, 27.57; H, 1.79; N, 6.93%. ^{1}H NMR (400 MHz, DMF-d_7, 298 K, ppm): δ 8.95 (s, 1H, C2-H), 7.98 (s, 1H, C5-H), 7.86–7.75 (m, 2H, C7-H, C11-H), 7.45–7.37 (m, 3H, C4-

H, C8-H, C10-H). ^{13}C NMR (101 MHz, DMF-d_7, 298 K, ppm): δ 163.3 (C9), 160.9 (2×C9), 138.1 (C2), 132.9 (C6), 130.7 (C4), 123.8 (C7,11), 119.6 (C5), 117.1 (C8), 116.8 (C10). ^{195}Pt NMR (86 MHz, DMF-d_7, 298 K, ppm): δ -3152. ESI+ MS (MeOH, *m/z*): 646.2 (calc. 646.3; 15%; $[PtI(L^6)_2]^+$), 706.1 (calc. 706.1; 25%; $\{[PtI_2(L^6)] + 4H_2O + Na^+\}^+$), 717.3 (calc. 717.5; 45%; $\{[PtI(L^6)_2] + 4H_2O\}^+$), 796.0 (calc. 796.2; 100%; $\{[PtI_2(L^6)_2] + Na^+\}^+$), 812.9 (calc. 812.4; 10%; $\{[PtI_2(L^6)_2] + K^+\}^+$). IR (ATR, ν, cm^{-1}): 468w, 543w, 614w, 643w, 738w, 803w, 837m, 966w, 1011w, 1063w, 1127w, 1149w, 1221m, 1304w, 1519s, 3110m.

cis-$[PtI_2(L^7)_2]$ (**7**): Yellow solid. Yield 88%. Anal. Calcd. for $C_{18}H_{14}I_2Cl_2N_4Pt$: C, 26.82; H, 1.75; N, 6.95%; found: C, 27.15; H, 1.84; N, 6.77%. ^{1}H NMR (400 MHz, DMF-d_7, 298 K, ppm): δ 8.99 (s, 1H, C2-H), 8.03 (s, 1H, C5-H), 7.86–7.74 (m, 2H, C7-H, C11-H), 7.69–7.57 (m, 2H, C8-H, 10-H), 7.42 (s, 1H, C4-H). ^{13}C NMR (101 MHz, DMF-d_7, 298 K, ppm): δ 138.0 (C2), 135.2 (C6), 133.3 (C9), 130.8 (C4), 130.2 (C8,10), 123.1 (C7,11), 119.4 (C5). ^{195}Pt NMR (86 MHz, DMF-d_7, 298 K, ppm): δ -3146. ESI+ MS (MeOH, *m/z*): 678.2 (calc. 677.9; 100%; $[PtI(L^7)_2]^+$), 843.7 (calc. 834.8; 15%; $\{[PtI_2(L^7)_2] + K^+\}^+$). IR (ATR, ν, cm^{-1}): 515w, 649w, 733w, 821m, 963w, 1011w, 1065w, 1094w, 1132w, 1184w, 1252w, 1307m, 1418w, 1516s, 3111m.

General methods

Electrospray ionization mass spectrometry (ESI-MS; methanol solutions) was carried out with an LCQ Fleet ion trap spectrometer (Thermo Scientific; QualBrowser software, version 2.0.7) in a positive (ESI+) ionization mode. ^{1}H and ^{13}C NMR spectroscopy and ^{1}H-^{13}C gs-HMQC and ^{1}H-^{13}C gs-HMBC two-dimensional correlation experiments were measured for DMF-d_7 solutions of complexes **1**–**7** at 298 K using a Varian spectrometer at 400.00 MHz (for ^{1}H NMR), 101.00 MHz (for ^{13}C NMR) and 86.00 MHz (for ^{195}Pt); gs = gradient selected, HMQC = heteronuclear multiple quantum coherence, HMBC = heteronuclear multiple bond coherence. ^{1}H and ^{13}C NMR spectra were calibrated against the residual signals of the solvent, while ^{195}Pt NMR chemical shifts were referenced to the signal of $K_2[PtCl_6]$ (δ = 0 ppm) in an external reference solution. The splitting of proton resonances in the reported ^{1}H spectra is defined as s = singlet, d = doublet, t = triplet, m = multiplet. A Jasco FT/IR-4700 spectrometer (Jasco, Easton, MD, USA) was used for the collection of the Fourier-transform infrared (FTIR) spectra of complexes in the range of 400–4000 cm^{-1} using the attenuated total reflection (ATR) technique on a diamond plate. Elemental analysis was performed by a Flash 2000 CHNS Elemental Analyzer (Thermo Scientific).

The determination of Pt was performed using ICP-MS (Agilent 7700x, Agilent Japan) in a He mode to overcome potential interferences. External calibration was applied, and internal standard correction used. Calibration solutions were prepared by diluting a multi elemental certified reference material – water calibration solution (obtained from Analytika Ltd., Czech Republic) with the concentration (100.0 ± 0.2) mg/L of each metal, including Pt. All samples were diluted accordingly with deionized water prior to ICP-MS analysis.

X-ray crystallography

Data collection and cell refinement of **3**, **4**, **5** and **7** were performed using a Stoe StadiVari (Stoe & Cie GmbH, Darmstadt, Germany) diffractometer using a Pilatus3R 300K detector and a microfocused X-ray source Incoatec IμS 2.0 HB (Ag Kα radiation). The multi-scan absorption corrections were applied using the program Stoe LANA software.[1] The structure was solved using SHELXT [67] or Superflip [68] program and refined by the full matrix least-squares procedure with Olex2.refine [69] using an aspherical model by the Hirshfeld Atom Refinement (HAR) method implemented in OLEX2 version 1.5-alpha [70]. The wave function was calculated using ORCA 4.2.0 software [71] with basis set x2c-TZVP [72] (for **3** and **4**) or ECP-def2-TZVP [73] (for **5** and **7**) and hybrid-exchange-correlation functional PBE0 [74]. The NoSpherA2 implementation [75] of HAR makes used for tailor-made aspherical atomic factors calculated on-the-fly from Hirshfeld-partitioned electron density. All non-hydrogen atoms were refined anisotropically. Hydrogen atoms of **3** were refined anisotropic using Rigid body (RIGU) restrains, while hydrogen atoms of others (**4**, **5** and **7**) were refined isotropic. The refinement of hydrogen atoms was performed with restraints on C–H distances from neutron diffraction data (1.083 Å for aromatic ring, 1.077 Å for methyl group, 1.092 Å for methylene group) [76]. The molecular structures and packing diagrams were drawn with MERCURY [77].

CCDC reference numbers 2211813 (**3**), 2211814 (**4**), 2211815 (**5**) and 2211816 (**7**) contain the supplementary crystallographic data for the X-ray studies reported in this work. Authors will release the atomic coordinates upon article publication.

Solution stability and interaction studies using ^{1}H NMR spectroscopy

The appropriate amounts of **1**–**7** for the preparation of 1 mM solutions were dissolved in 250 μL of DMF-d_7 and 250 μL of PBS in D_2O (pH 7.4). *Note*: DMF-d_7 ensured solubility of all the tested complexes, as their solubility in water is only very low. ^{1}H NMR spectra of the prepared solutions were recorded in various time intervals (0–24 h) and incubated at ambient temperature between individual experiments. The obtained ^{1}H NMR spectra were referenced to the residual signal of H_2O (4.79 ppm). ^{1}H NMR spectra of the free ligands L^1–L^7 were also recorded under the same experimental conditions. The stability of **1**–**7** was evaluated by determining the amount of the complexes in solution by integrating a representative C2–*H* signal in the obtained ^{1}H NMR spectra.

GSH (2 mol equiv.) was added to the solutions of complexes **1**–**7** (1 mM) in 250 μL of DMF-d_7 and 250 μL of PBS in D_2O (pH 7.4). ^{1}H NMR spectra of the prepared solutions were recorded at various time points (0–24 h) and incubated at ambient temperature between the individual experiments. Analogical ^{1}H NMR experiments were performed for the mixtures of **6** and **7** (and cisplatin for comparative purposes) with 2 mol equiv. of GMP in 50% DMF-d_7/50% D_2O.

Lipophilicity studies (log P)

Octanol-saturated water (OSW) and water-saturated octanol (WSO) were prepared from *n*-octanol and 0.2 M water solution of KI by overnight stirring. Stock solutions were prepared by ultrasonication (5 min) and shaking (30 min) of 1 μmol of **1**–**7** in 11 mL of OSW. After that, the mixtures were centrifuged (5 min, 11,000 rpm) and the supernatants were collected. 5 mL of the OSW solution was analyzed by ICP-MS to determine the Pt concentration ($[Pt]_{OSWb}$; obtained values were corrected for the adsorption effects) and other 5 mL of the OSW solution was added to 5 mL of WSO and shaken at ambient temperature for 2 h. After that, the mixture was centrifuged, and the aqueous layer was also analyzed by ICP-MS ($[Pt]_{OSWa}$). log P = log($[Pt]_{WSO}/[Pt]_{OSWa}$) equation was used for the partition coefficient calculation, where $[Pt]_{WSO} = [Pt]_{OSWb} - [Pt]_{OSWa}$.

HPLC purity check

Reversed-phase high-performance liquid chromatography (RP-HPLC) coupled to ESI+ MS was performed on a UHPLC-MS device (Dionex/Thermo Fisher Scientific) equipped with an Acclaim 120 (C18 stationary phase; 5 μm pore size, 120 Å, 2.1 × 50 mm). The mixture of H_2O (A) and MeCN (B) was used as the mobile phase at the gradients of 20 % B (t = 0 min), 80 % B (t = 15 min), 80 % B (t = 20 min), 20 % B (t = 21 min) and 20 % B (t = 30 min) over a 30 min period (0.4 mL min^{-1} flow rate). The detection wavelength was 254 nm.

Cell cultures

Human prostate cancer DU-145 (ATCC HTB-81), human liver hepatocellular carcinoma HepG2 (ATCC HB-8065), human breast cancer MCF-7 (ATCC HTB-22), myeloma U266B1 (U266; ATCC ®TIB-196™) and human bone marrow stromal HS-5 (CRL-11882) cell lines were purchased from ATCC (American Type Culture Collection, Manassas, VA, USA). Myeloma KMS12-PE (JCRB0430) cell line was obtained from JCRB – Japanese Cancer Research Resources Bank (National Institute of Biomedical Innovation, Osaka, Japan).

The cells were cultured in standard conditions (37 °C, 5% CO_2), using suitable culture media, i.e. DMEM F-12HAM (Dulbecco's Modified Eagle Medium: Nutrient Mixture F-12) for DU-145 cells, and EMEM (Eagle's Minimum Essential Medium) for HepG2 and MCF-7 cells. The culture media were supplemented with 10% FBS, and antibiotics (1% streptomycin/penicillin mixture), whereas the experiments were conducted in culture media with a reduced content of FBS (2.5%). Human fibroblast HS-5 and two human myeloma U266B1 and KMS12-PE cell lines were maintained in RPMI 1640 medium supplemented with 10% (KMS12-PE) and 15% (U266B1) FBS, antibiotics (1% streptomycin/penicillin mixture), 1% L-glutamine, and 100 mM sodium pyruvate in standard conditions.

Co-culture of KMS12-PE myeloma cell line and HS-5 fibroblast cell line were cultured under the same conditions as the co-culture of U266B1 myeloma cell line and HS-5 (15%

FBS), but only with 10% FBS. A ratio of myeloma cells (KMS12-PE or U266B1) and HS-5 fibroblasts was 20:1.

In vitro cytotoxicity

Cells were seeded in 96-well plates at an initial density of 5,000 cells per well. Cells were cultured in standard conditions for 24 h and then **1**–**7** were administered at different concentrations (i.e. 1.0 μM for DU-145, HepG2 and MCF-7 cells, and 1–3 μM for U266B1 and KMS12-PE multiple myeloma cells) for the next 24 h. Next, 10 μL of MTT dye (Sigma-Aldrich, Darmstadt, Germany) was added to each well and after 3-4 h of incubation (37 °C, 5% CO_2) the medium was aspirated and formazan produced in the cells appeared as dark crystals at the bottom of the wells. Then formazan crystals were dissolved in a DMSO (Sigma–Aldrich, Darmstadt, Germany) for DU-145, HepG2 and MCF-7, or 10% SDS solution for HS-5, U266B1, and KMS12-PE, and absorbance was measured at 570 nm (SpectraMax® iD3, Molecular Devices, San Jose, CA, USA). Experiments were conducted in triplicates. The resulting values represent mean percentage of viability (in the percent of control). Cisplatin was used as a reference drug. DMF (Sigma–Aldrich, Darmstadt, Germany) was used as a solvent for stock solutions of the studied complexes. For fibroblast HS-5 and myeloma U266B1 and KMS12-PE cell lines, RPMI-1640 medium supplemented with 10% (KMS12-PE) or 15% (for U266B1) FBS was used as a negative control. Experiments were conducted two times in three repetitions for each condition.

Data from the cytotoxicity assays were analyzed using Mann–Whitney U test with GraphPad Prism 4.0 Software (GraphPad Software Inc., San Diego, CA, USA). Values of $p < 0.05$ were considered to be statistically significant.

Assessment of cell apoptosis

The Annexin-V/PI staining was carried out to semi-quantify the viable, apoptotic, and necrotic cells after 24 h treatment of the used concentrations of **6**. Untreated cells cultivated with 10 % DMSO were used as a control sample. For determination of apoptosis by Annexin-V/PI, cells were harvested after 24 h, centrifuged, and kept continuously on ice. Binding buffer (140 mM NaCl, 4 mM KCl, 0.75 mM $MgCl_2$ and 10 mM HEPES in DDW), Annexin V, 7-AAD and $CaCl_2$ were added sequentially. The samples were incubated on ice for 15 min without the presence of light.

For determination of apoptosis by caspase 3 and 7 activities, cells were harvested after 24 h, centrifuged and kept on ice. Binding buffer and 2 % FBS was added. Subsequently, the CellEvent ™ Caspase-3/7 Green Detection Reagent was added at a final concentration of 500 nM. Samples were incubated at room temperature for 40 min without light. Finally, DAPI was added and incubated for 5 min without the presence of light.

For both methods, at least 10,000 cells per sample were analyzed. Apoptosis was analyzed by flow cytometry (BD FACSVerse, BD, USA), and the collected data was processed using BD FACSuite (BD).

Cell cycle analysis

Cell cycle analysis was performed using flow cytometry with PI to stain cellular DNA. Cells were treated for 24 h with the used concentrations of **6**, harvested and fixed with 96% ice-cold ethanol at -20 °C. After cell washing with ice cold PBS + 2% FBS, incubation with 0.2 mg/mL RNAse A + PBS at room temperature (RT) for 30 min was carried out. After that, 200 µL of PI was added and the cells were analyzed by BD FACSVerse flow cytometry (BD, USA). The results were analyzed using BD FACSuite (BD) software.

Cellular accumulation

The U266B1, KMS12-PE and HS-5 cells were seeded in 6-well culture plates at a density of 1×10^6 (U266B1, KMS12-PE) or 1×10^5 (HS-5) cells per well and incubated overnight (37 °C and 5% CO_2 in a humidified incubator). Then, the cells were treated for 24 h by 1 µM concentration of complex **6**. Then the cells were washed with PBS (2 × 2 mL), harvested by the trypsinization, centrifuged and the obtained cell pellets were stored on ice. After that, the cells were digested in 500 µL of nitric acid (6 h, 70 °C), to give the fully homogenized solutions. The solutions were 25× diluted with water and the metal content was determined by ICP-MS. The obtained values were corrected for adsorption effects.

DNA interaction in a cell-free medium

10 ml of the mixtures of complex **6** or **7** (and cisplatin for comparative purposes; 20 µM final concentration for all compounds) with salmon sperm DNA (64 µg/mL final concentration) in 10 mM sodium perchlorate was stirred for 24 h at 37 °C. The mixtures were gel-filtrated through Sephadex G-25 columns, which were centrifuged for 5 min at 2,500 rpm. The obtained filtrates were subjected to UV-Vis spectroscopy (to determine the DNA concentration after the filtration) and ICP-MS (to determine the Pt content).

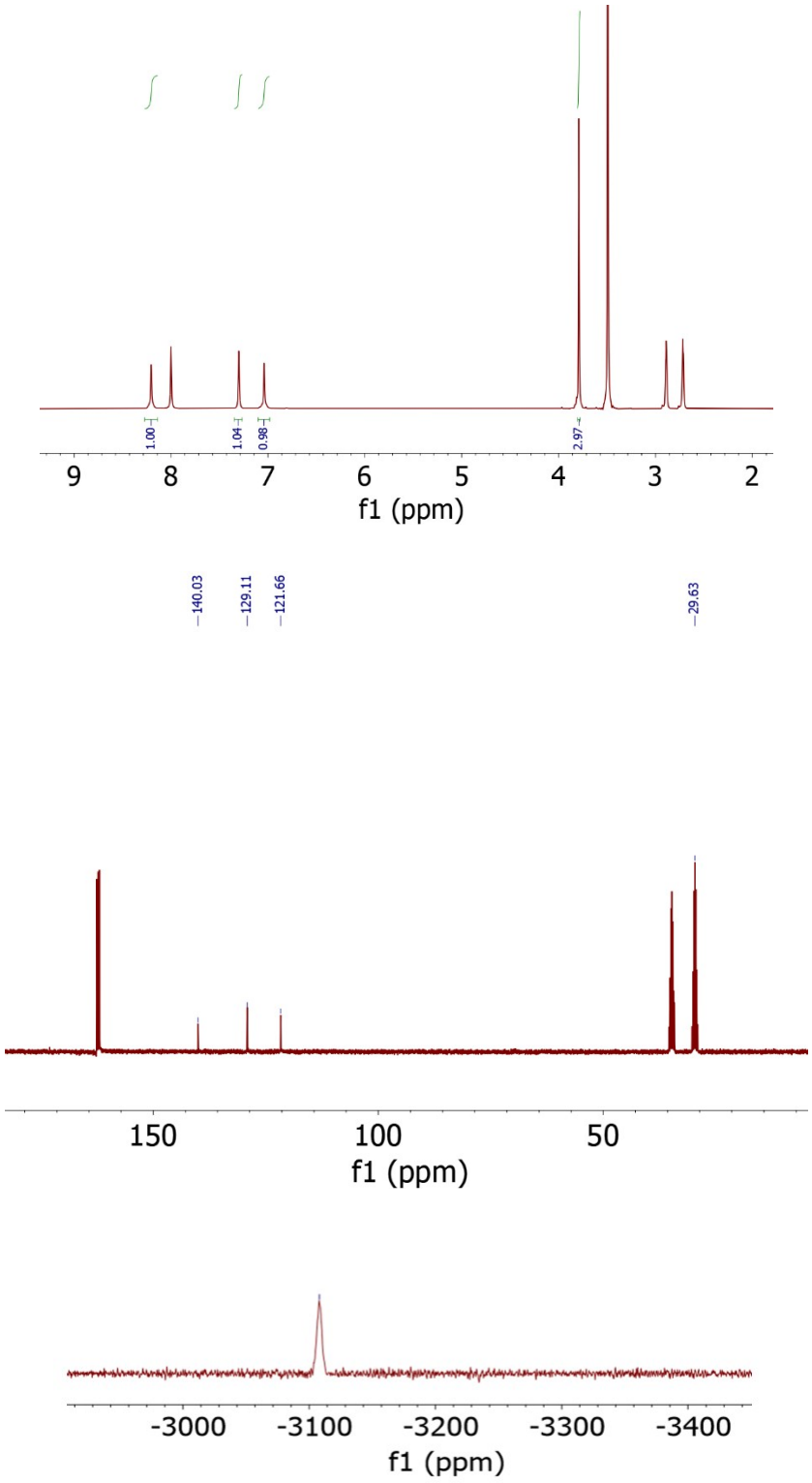

Figure S1. ^{1}H (*top*), ^{13}C (*middle*) and ^{195}Pt (*bottom*) NMR spectra of complex **1** in DMF-d_7.

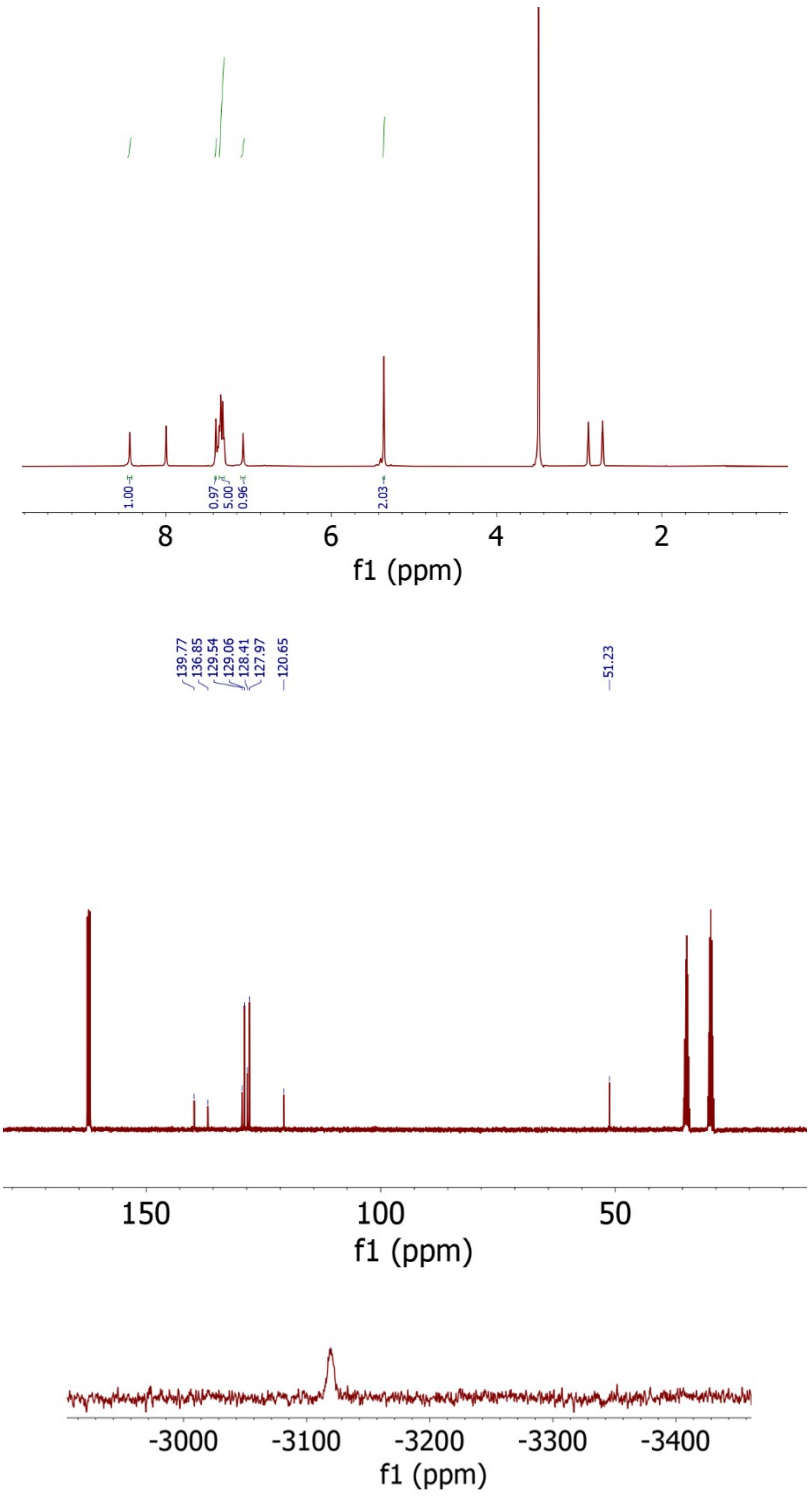

Figure S2. ^{1}H (*top*), ^{13}C (*middle*) and ^{195}Pt (*bottom*) NMR spectra of complex **2** in DMF-d_7.

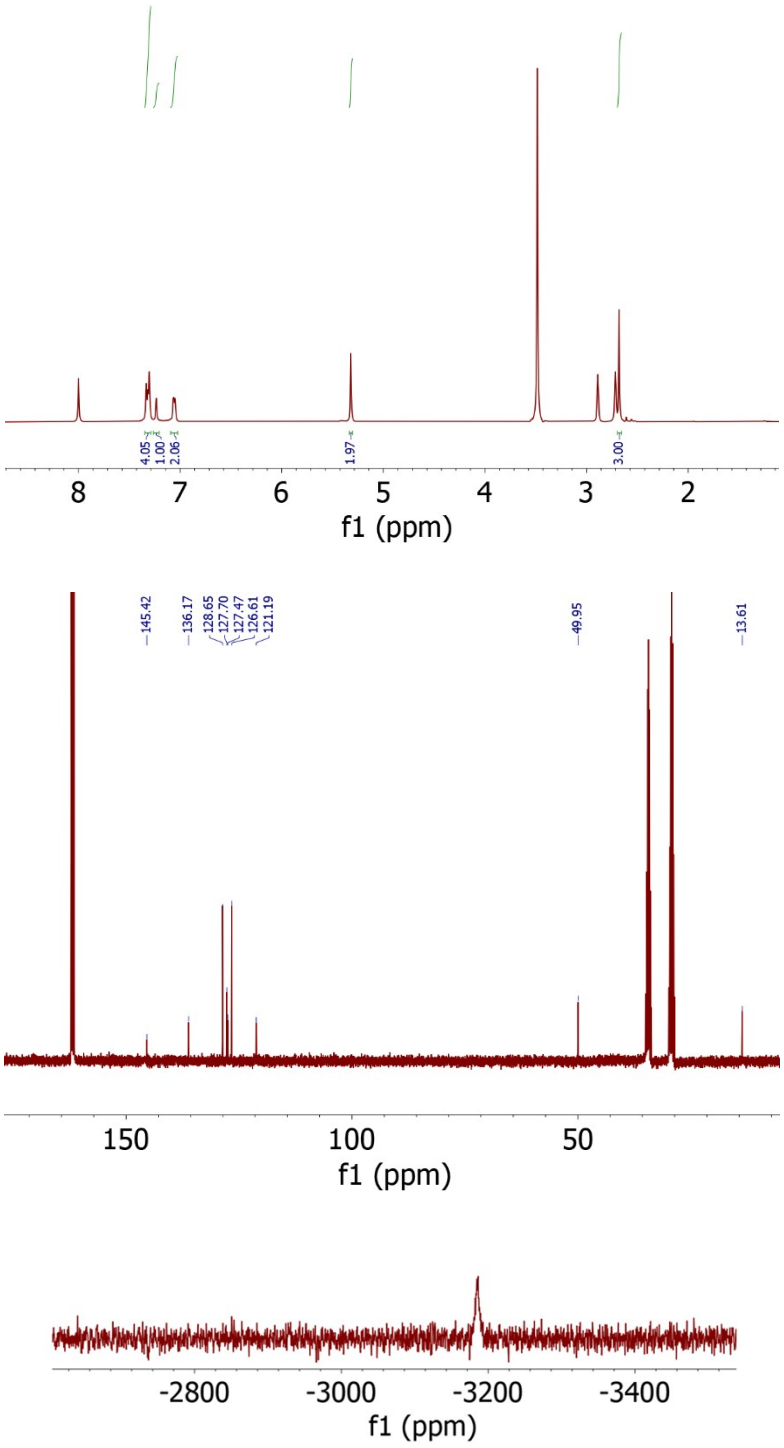

Figure S3. ^{1}H (*top*), ^{13}C (*middle*) and ^{195}Pt (*bottom*) NMR spectra of complex **3** in DMF-d_7.

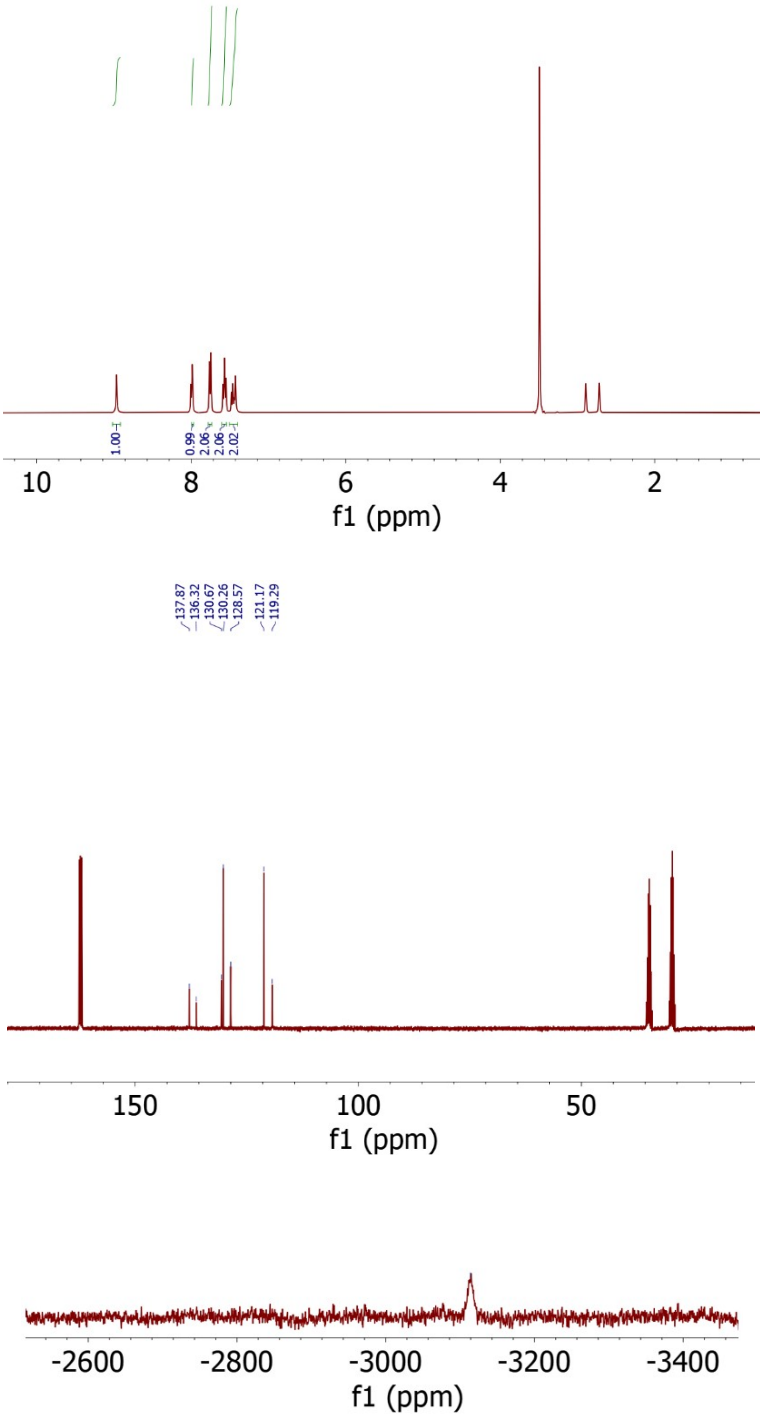

Figure S4. ^{1}H (*top*), ^{13}C (*middle*) and ^{195}Pt (*bottom*) NMR spectra of complex **4** in DMF-d_7.

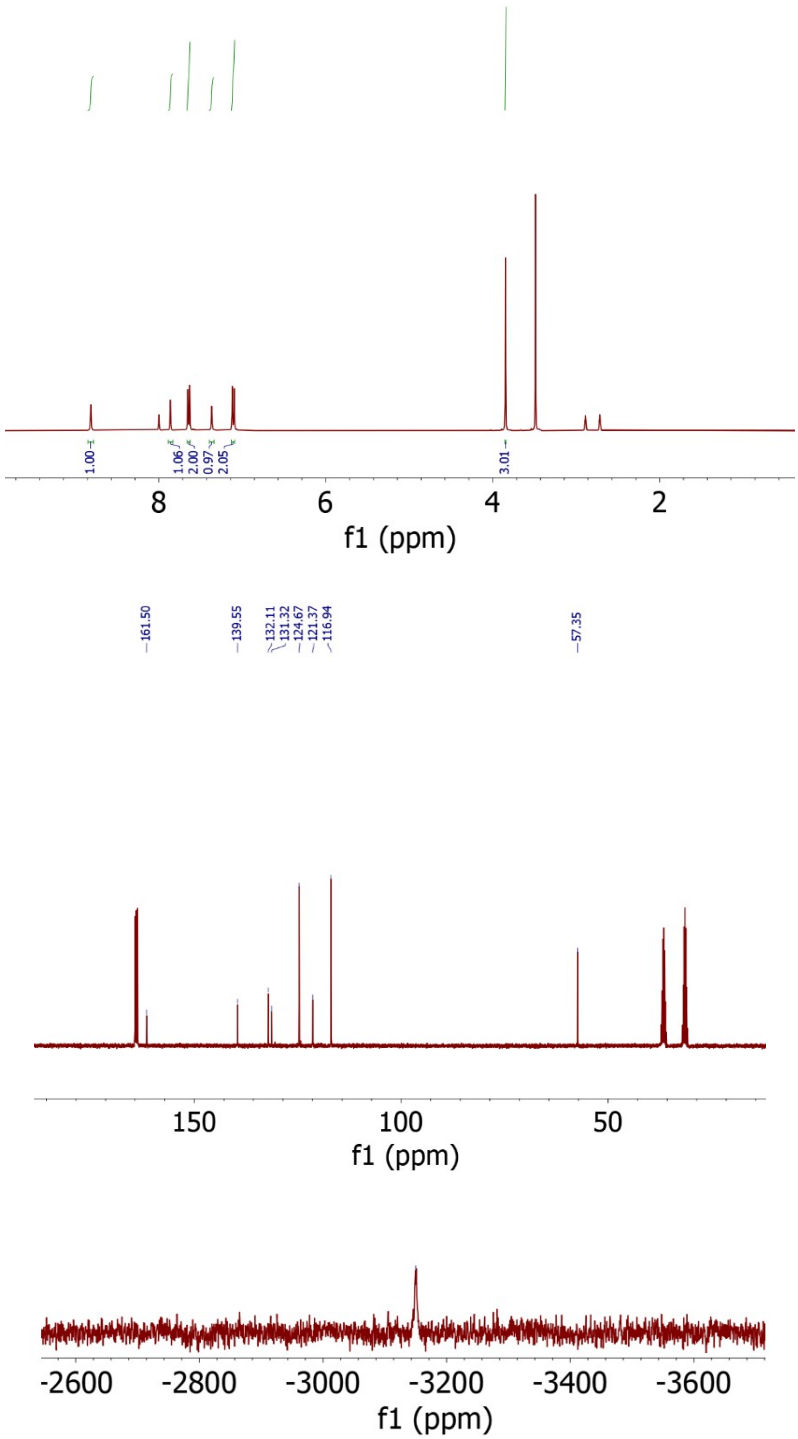

Figure S5. ^{1}H (*top*), ^{13}C (*middle*) and ^{195}Pt (*bottom*) NMR spectra of complex **5** in DMF-d_7.

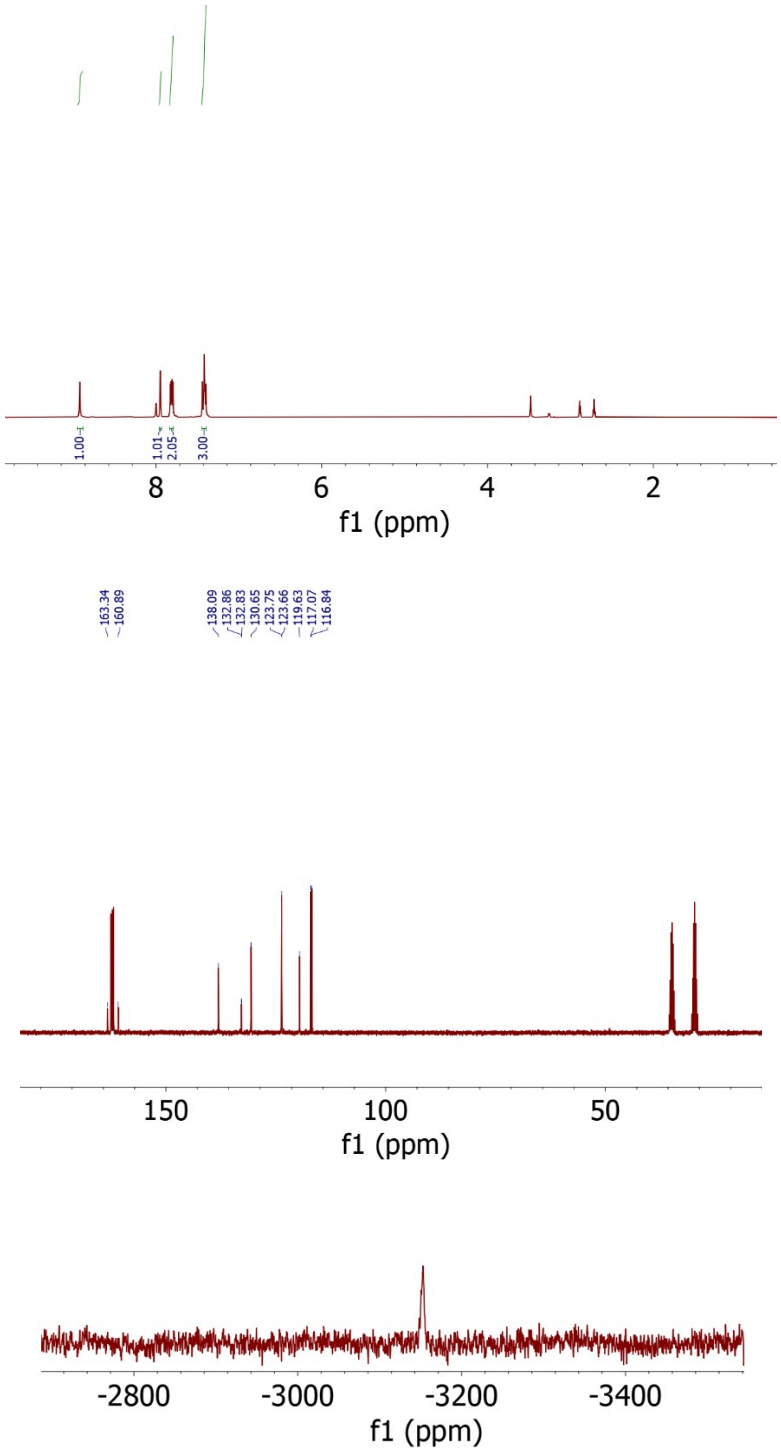

Figure S6. ^{1}H (*top*), ^{13}C (*middle*) and ^{195}Pt (*bottom*) NMR spectra of complex **6** in DMF-d_7.

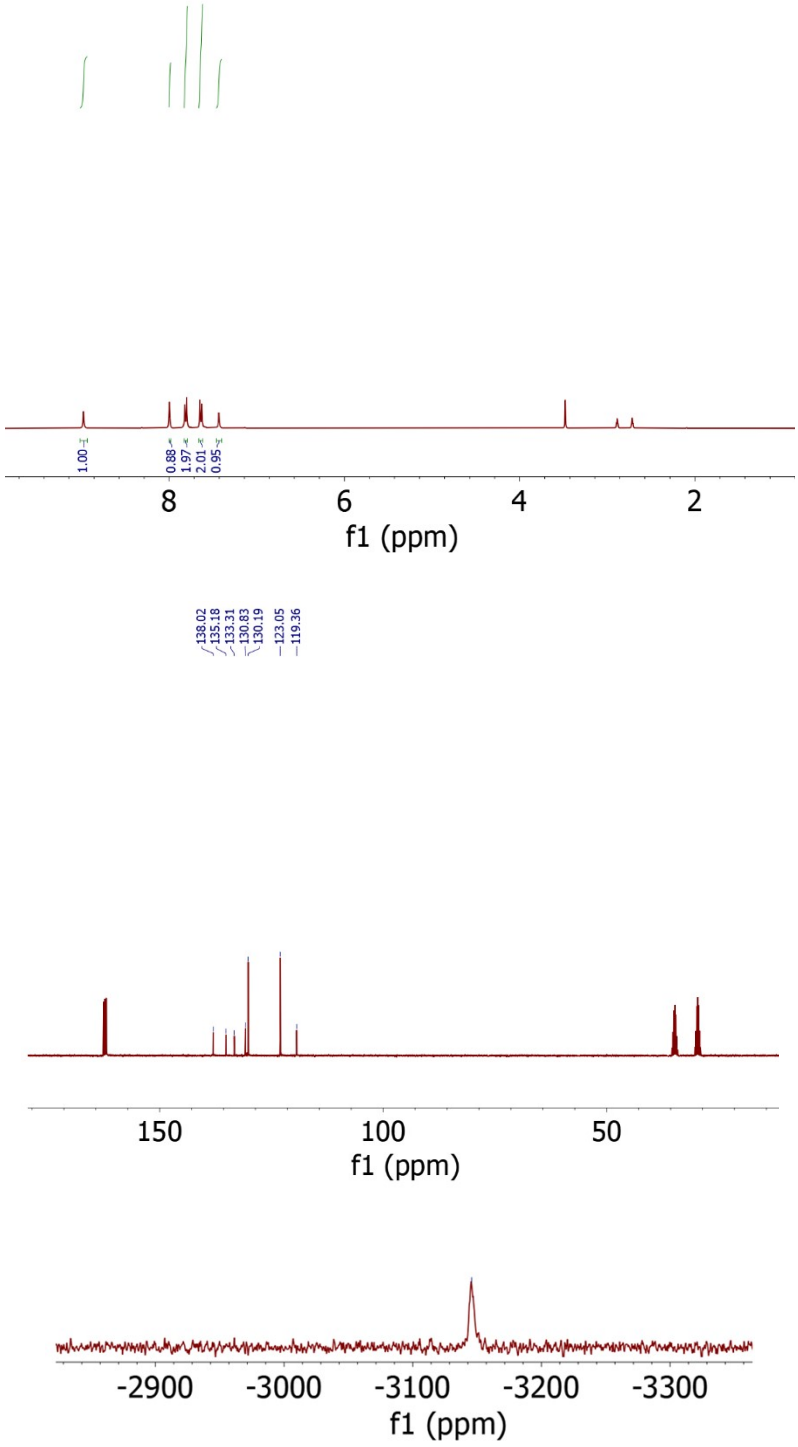

Figure S7. ^{1}H (*top*), ^{13}C (*middle*) and ^{195}Pt (*bottom*) NMR spectra of complex **7** in DMF-d_7.

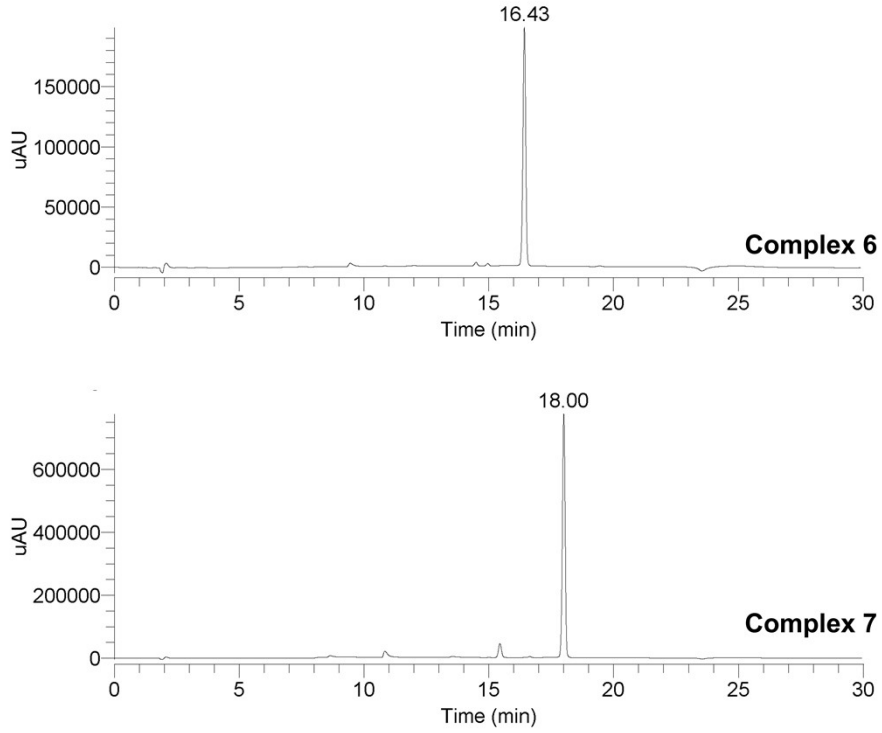

Figure S8. HPLC traces of the representative complexes **6** and **7**.

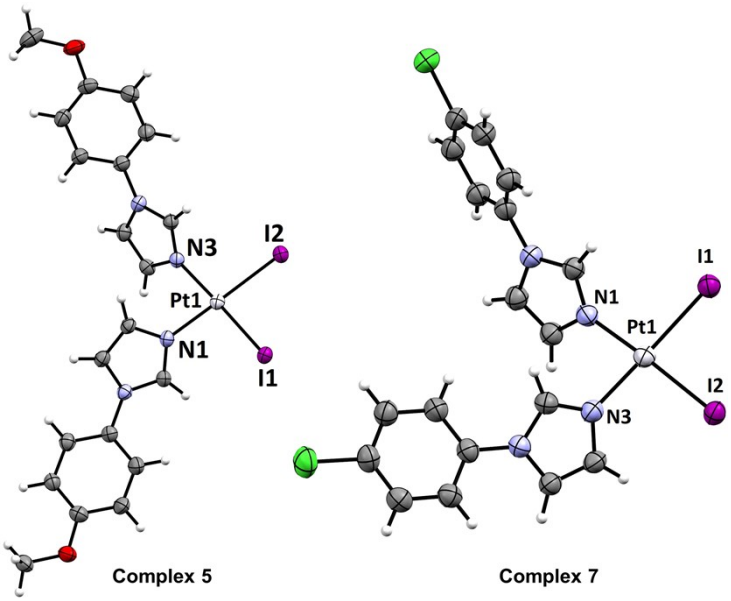

Figure S9. An Ortep drawing (50% probability level) of the complex molecules in compounds **5** and **7**. Colour code: C (grey), Cl (green), H (white), I (purple), N (blue), O (red) and Pt (light grey). Crystal structures of **5** and **7** contain two complex molecules in their asymmetric unit. For the sake of clarity only one of them was shown here.

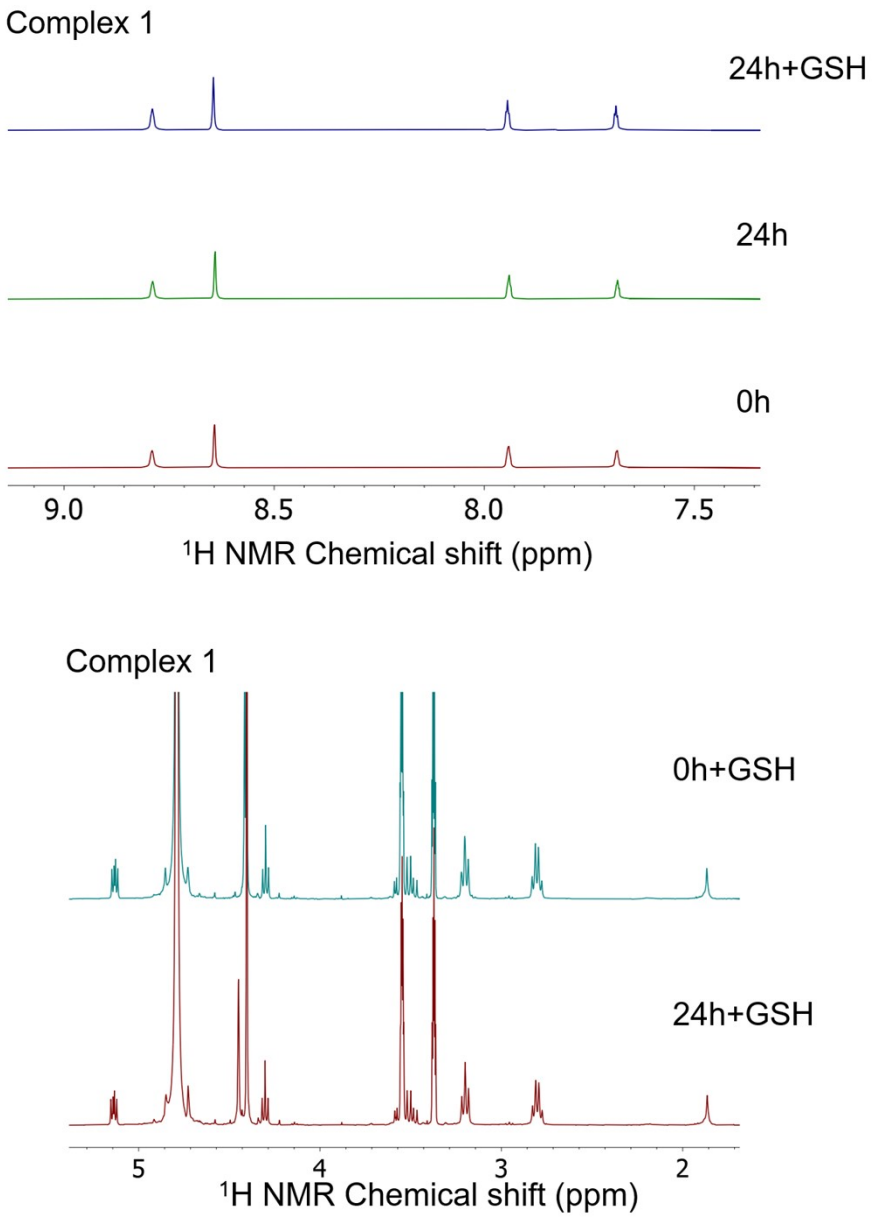

Figure S10. ^{1}H NMR studies of complex **1** in 50% DMF-d_7/50% of PBS in D_2O and in 50% DMF-d_7/50% of PBS in D_2O with 2 molar equiv. of reduced glutathione (GSH), as observed at different time points (0 h or 24 h).

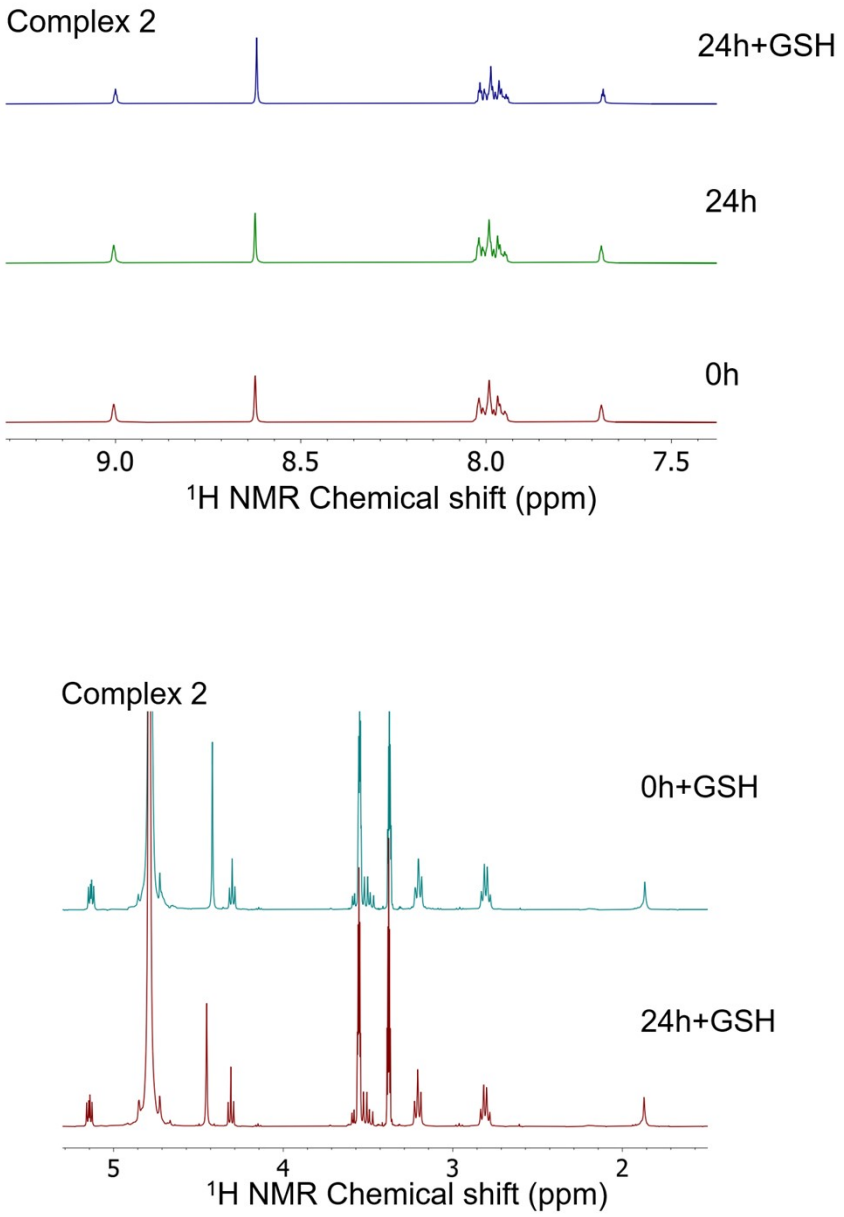

Figure S11. ^{1}H NMR studies of complex **2** in 50% DMF-d_7/50% of PBS in D_2O and in 50% DMF-d_7/50% of PBS in D_2O with 2 molar equiv. of reduced glutathione (GSH), as observed at different time points (0 h or 24 h).

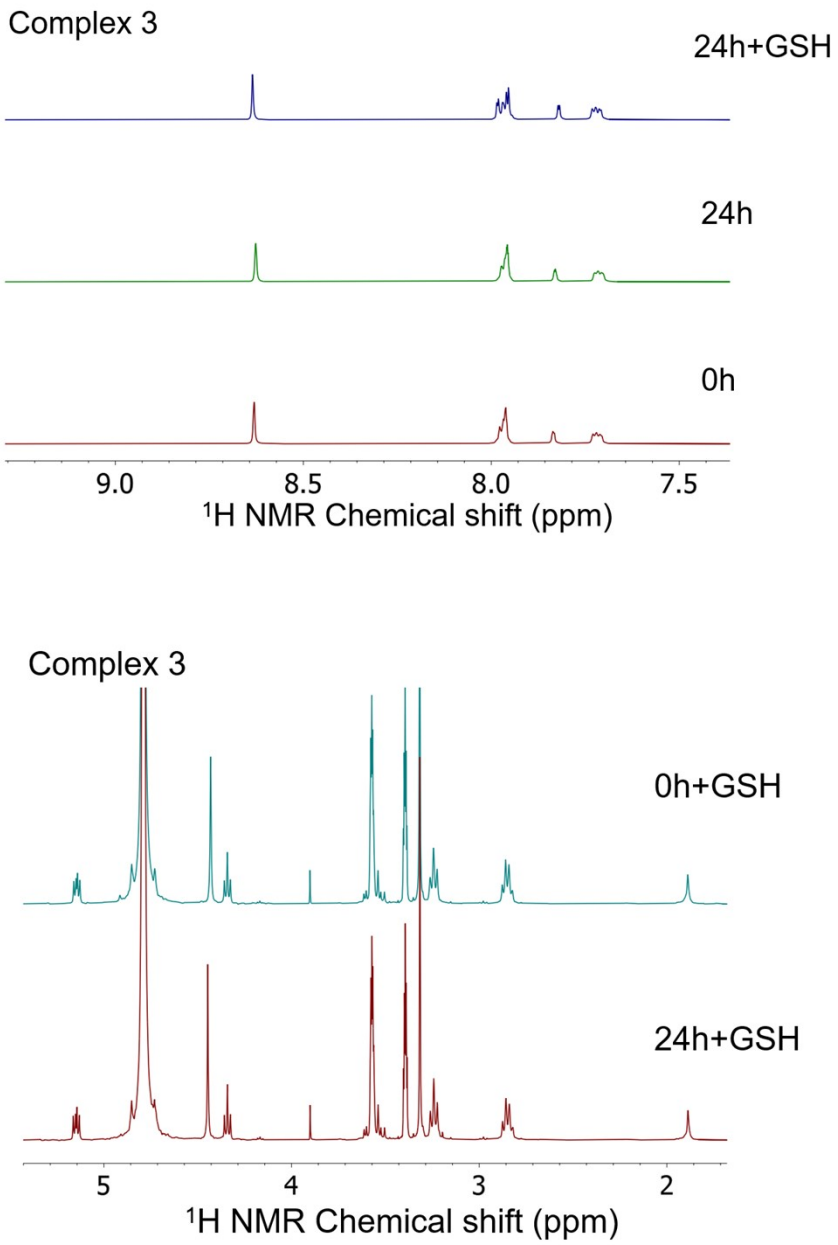

Figure S12. ^{1}H NMR studies of complex **3** in 50% DMF-d_7/50% of PBS in D_2O and in 50% DMF-d_7/50% of PBS in D_2O with 2 molar equiv. of reduced glutathione (GSH), as observed at different time points (0 h or 24 h).

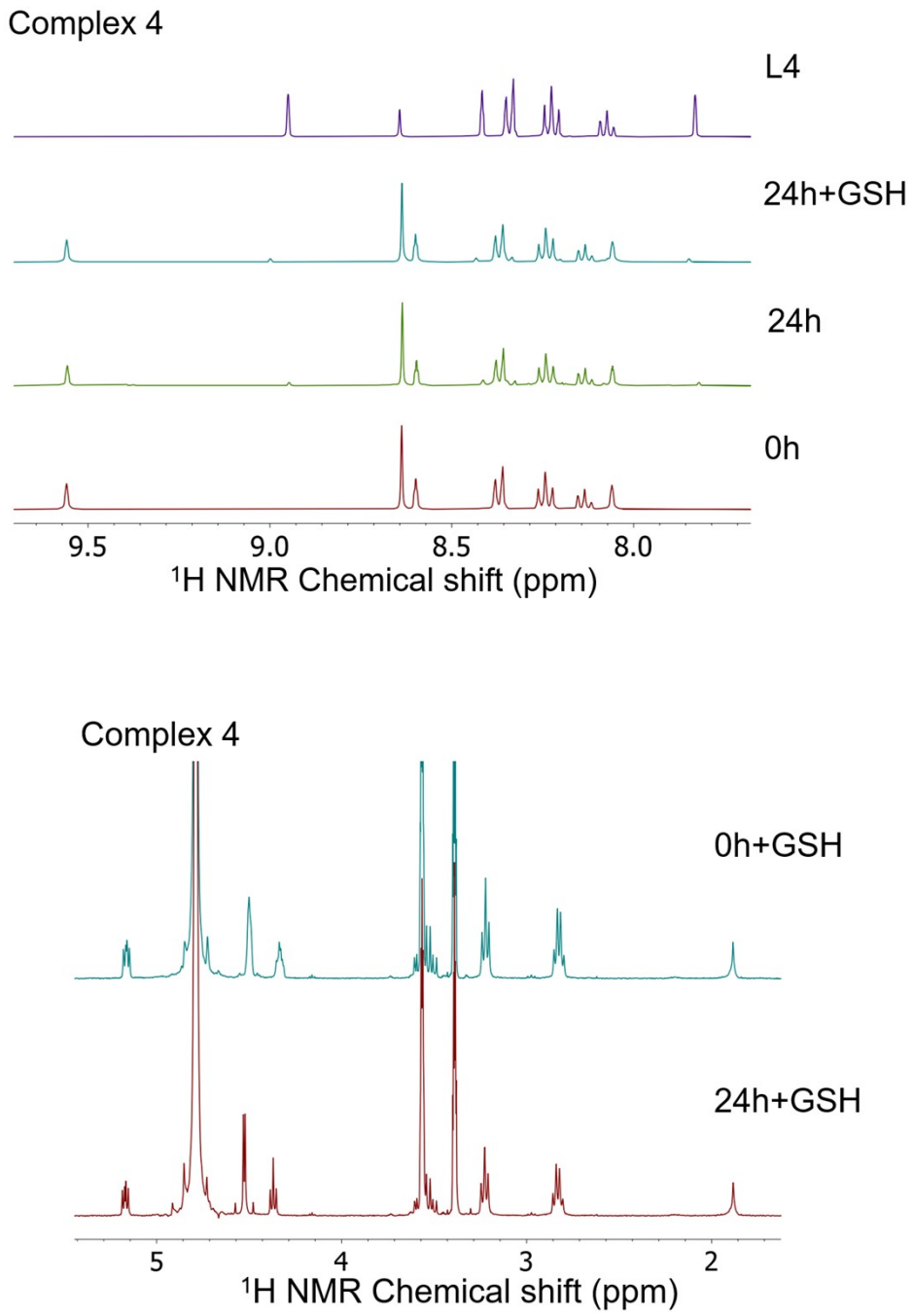

Figure S13. ^{1}H NMR studies of complex **4** in 50% DMF-d_7/50% of PBS in D_2O and in 50% DMF-d_7/50% of PBS in D_2O with 2 molar equiv. of reduced glutathione (GSH), as observed at different time points (0 h or 24 h).

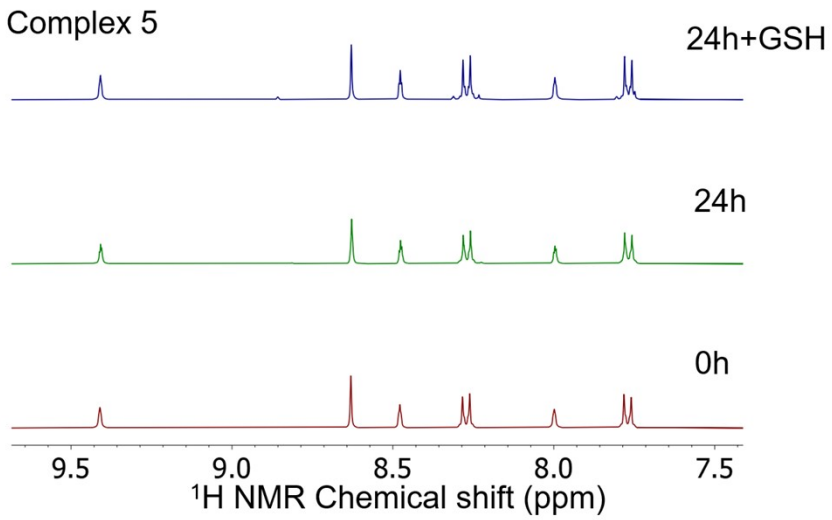

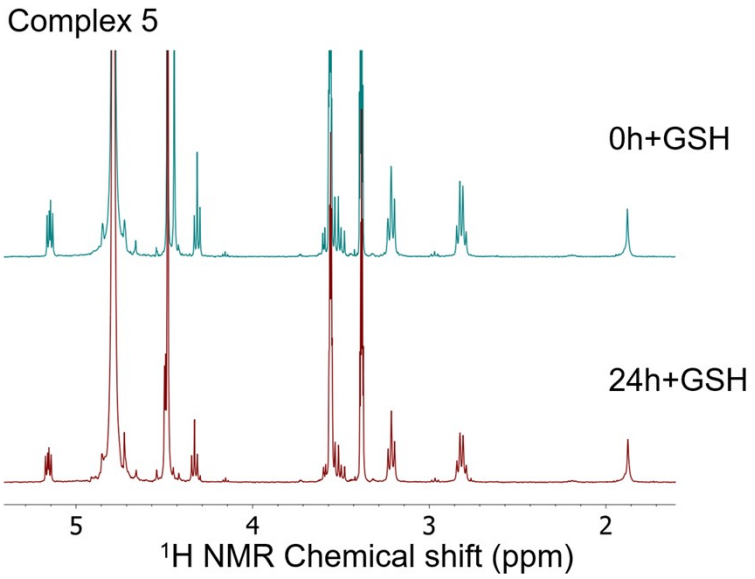

Figure S14. ^{1}H NMR studies of complex **5** in 50% DMF-d_7/50% of PBS in D_2O and in 50% DMF-d_7/50% of PBS in D_2O with 2 molar equiv. of reduced glutathione (GSH), as observed at different time points (0 h or 24 h).

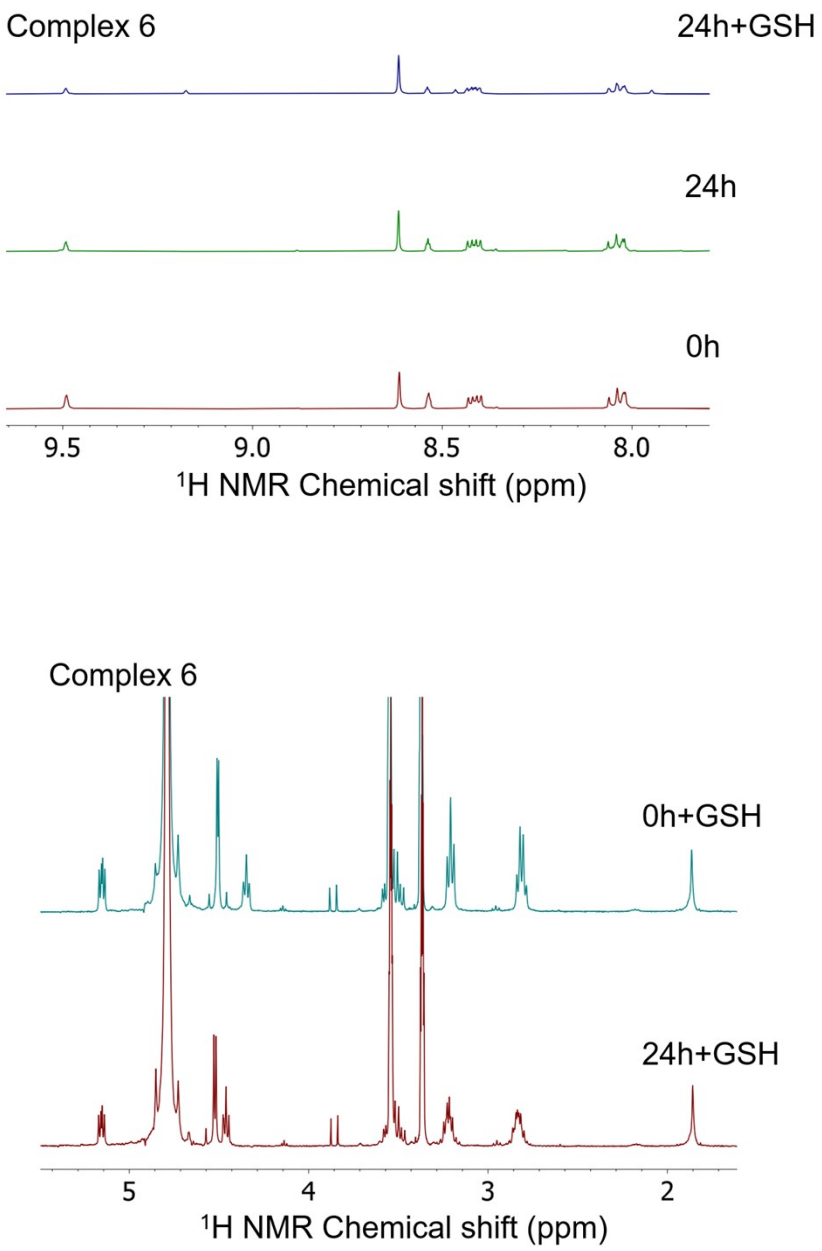

Figure S15. ^{1}H NMR studies of complex **6** in 50% DMF-d_7/50% of PBS in D_2O and in 50% DMF-d_7/50% of PBS in D_2O with 2 molar equiv. of reduced glutathione (GSH), as observed at different time points (0 h or 24 h).

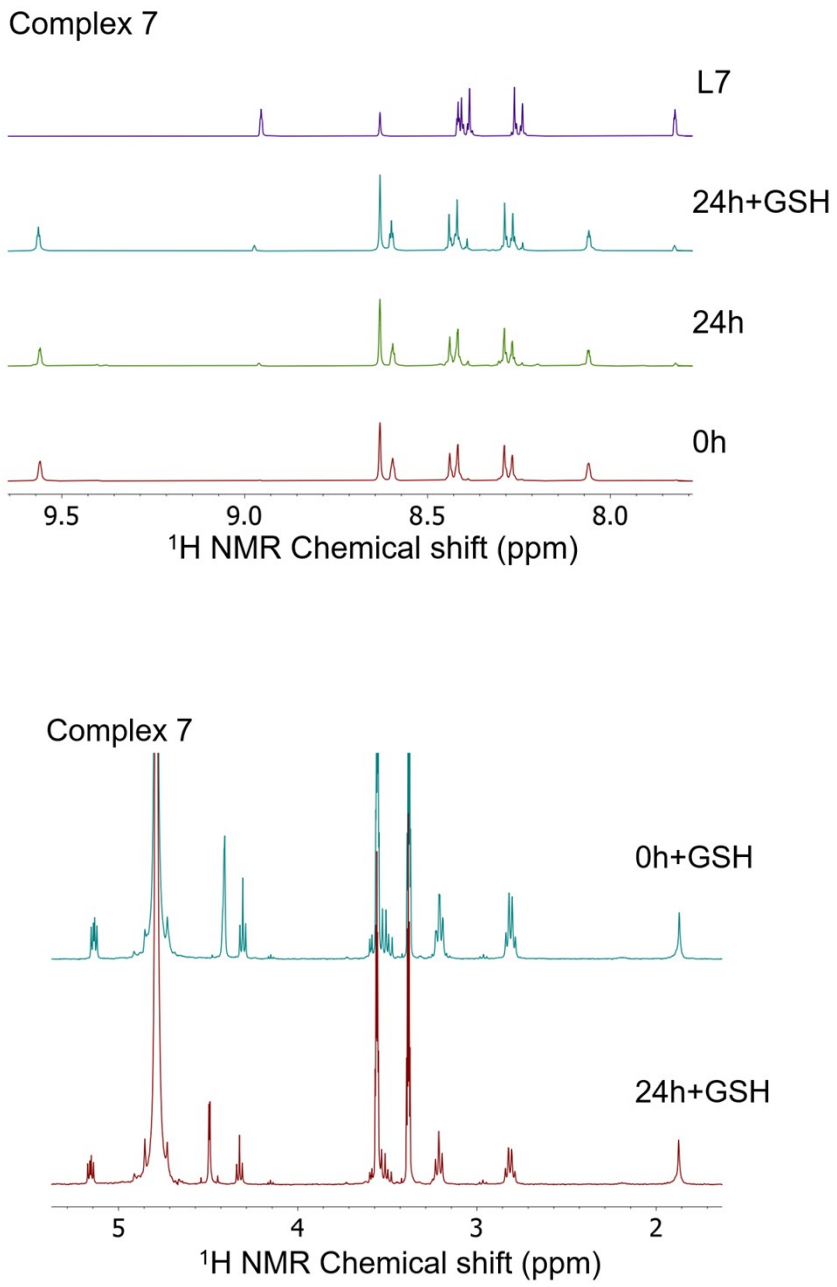

Figure S16. ^{1}H NMR studies of complex **7** in 50% DMF-d_7/50% of PBS in D_2O and in 50% DMF-d_7/50% of PBS in D_2O with 2 molar equiv. of reduced glutathione (GSH), as observed at different time points (0 h or 24 h).

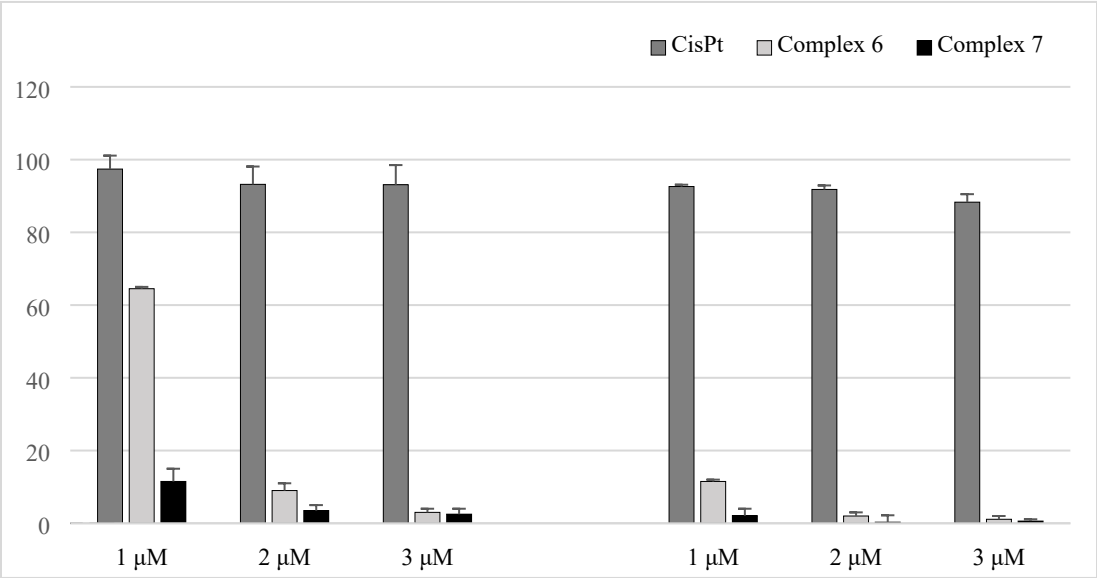

Figure S17. Cell viability of U266B1 (*left*) and KMS12-PE (*right*) myeloma cell lines after the treatment with complexes **6** and **7**, and the reference drug cisplatin (CisPt); MTT assay, 24 h exposure time.

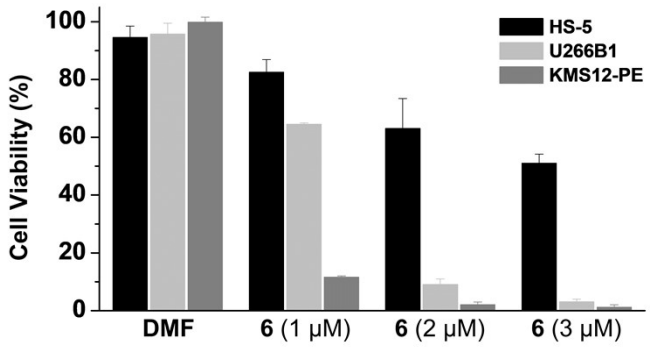

Figure S18. Cell viability of HS-5 stromal fibroblasts and myeloma cells (U266B1, KMS12-PE) after the treatment with complex **6**.

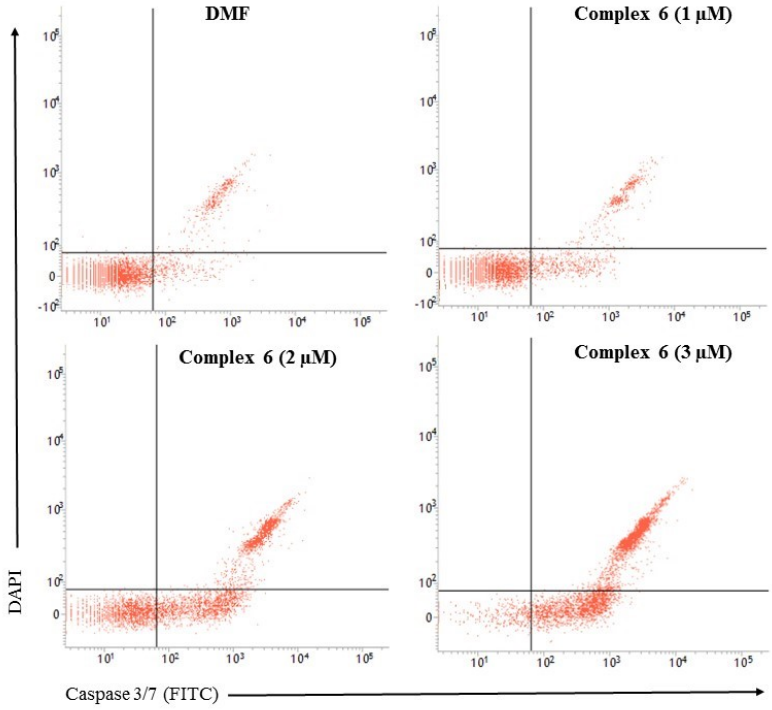

Figure S19. Apoptosis studies by determination of caspase 3/7 activities to semi-quantify viable, apoptotic and necrotic U266 myeloma cells after the 24 h treatment with 1 µM, 2 µM and 3 µM concentrations of complex **6**.

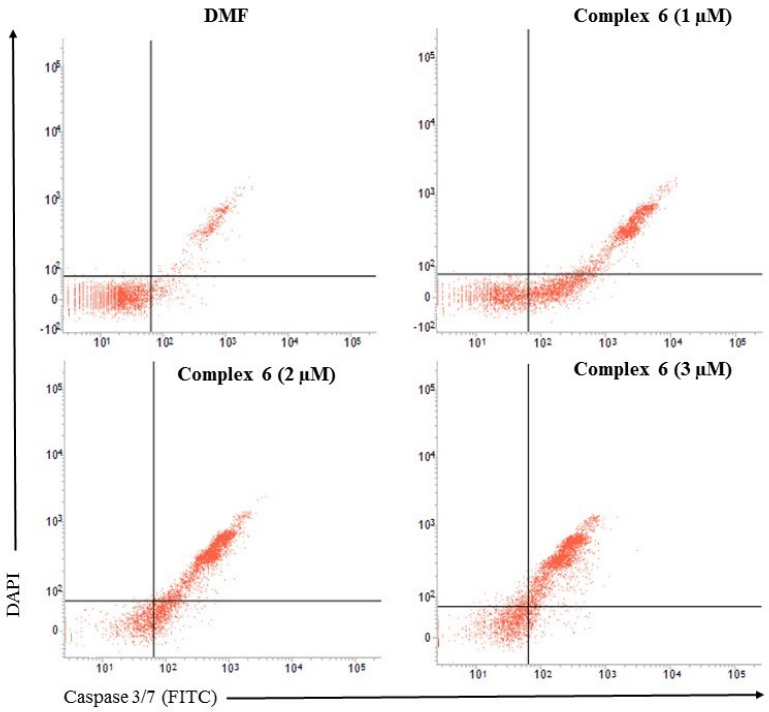

Figure S20. Apoptosis studies by determination of caspase 3/7 activities to semi-quantify viable, apoptotic and necrotic KMS12-PE myeloma cells after the 24 h treatment with 1 µM, 2 µM and 3 µM concentrations of complex **6**.

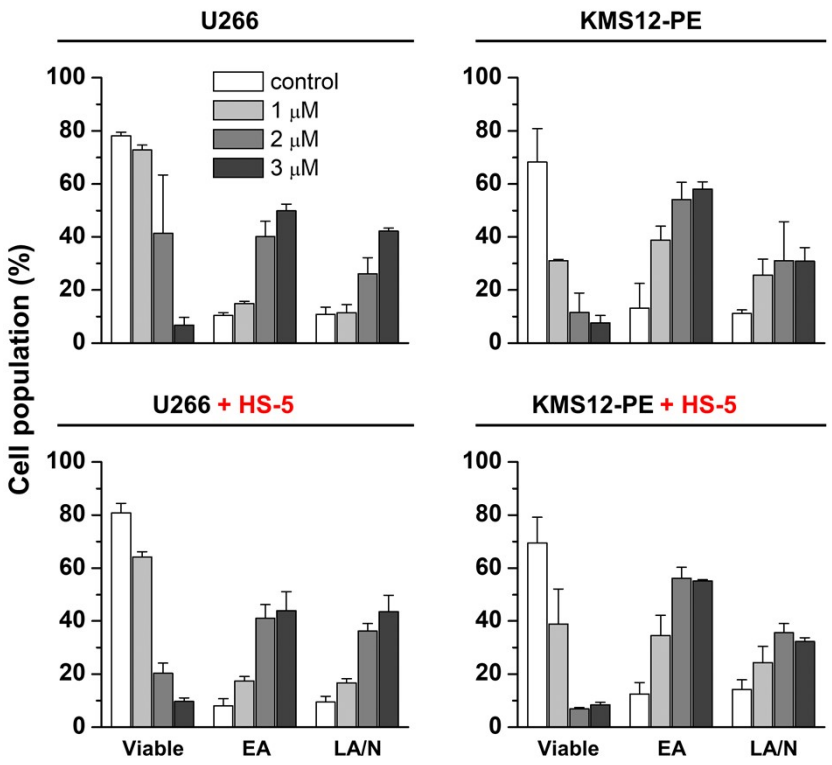

Figure S21. Apoptosis studies (Annexin-V/7-AAD staining) to semi-quantify viable, early apoptotic (EA) and late apoptotic/necrotic (LA/N) U266B1 and KMS12-PE myeloma cells or their co-cultures with HS-5 stromal fibroblasts, as detected after 24 h treatment with 1–3 μM concentrations of complex **6**.

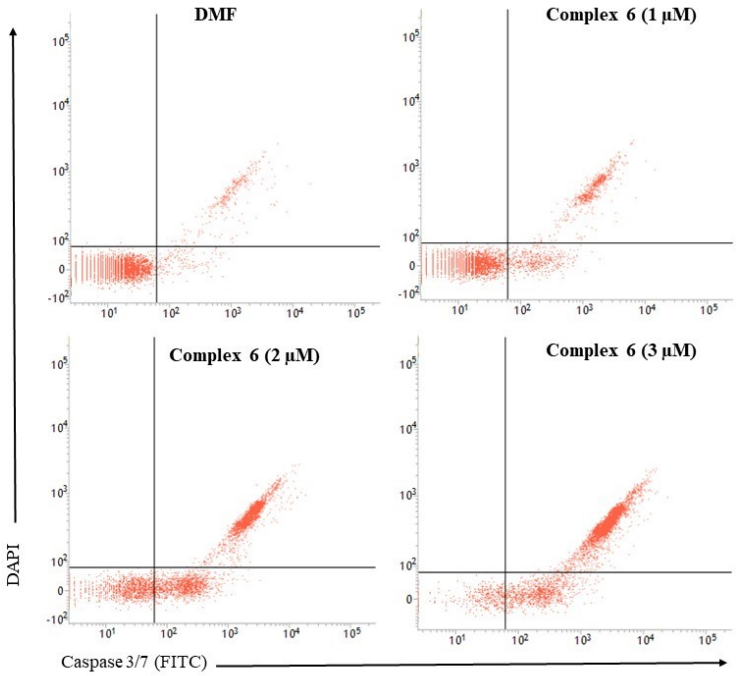

Figure S22. Apoptosis studies by determination of caspase 3/7 activities to semi-quantify viable, apoptotic and necrotic U266 myeloma cells co-cultured with the HS-5 stromal fibroblasts and treated for 24 h with 1 µM, 2 µM and 3 µM concentrations of complex **6**.

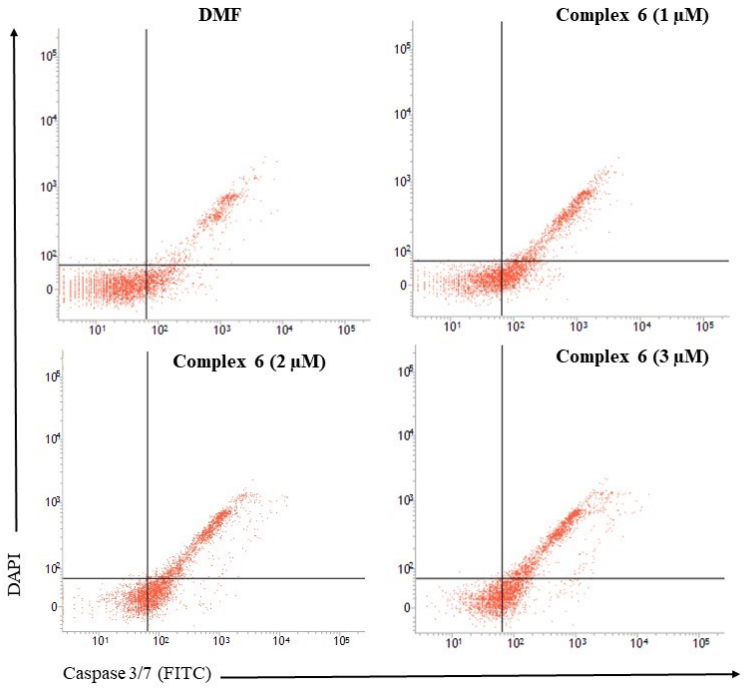

Figure S23. Apoptosis studies by determination of caspase 3/7 activities to semi-quantify viable, apoptotic and necrotic KMS12-PE myeloma cells co-cultured with the HS-5 stromal fibroblasts and treated for 24 h with 1 µM, 2 µM and 3 µM concentrations of complex **6**.

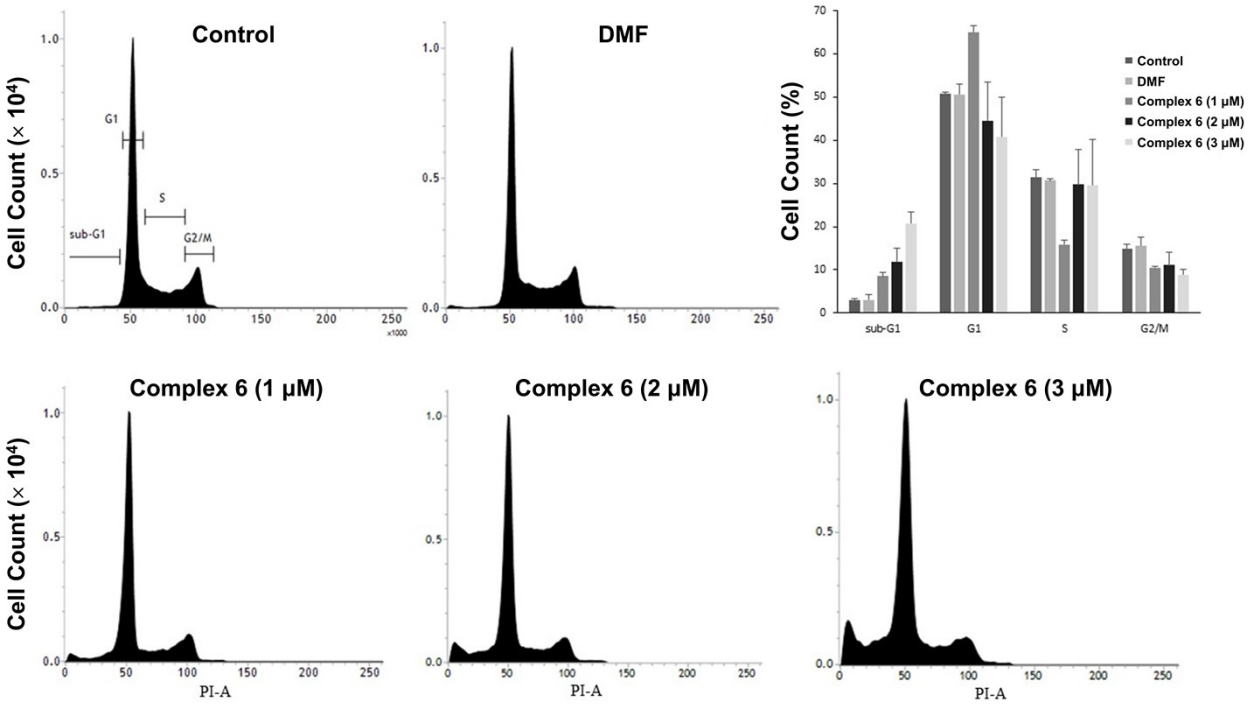

Figure S24. The cell cycle analysis in U266B1 myeloma cell line after 24 h treatment with 1–3 μM concentrations of **6**. Ctrl = medium, DMF = medium with DMF (the same concentration as for experiments with **6**).

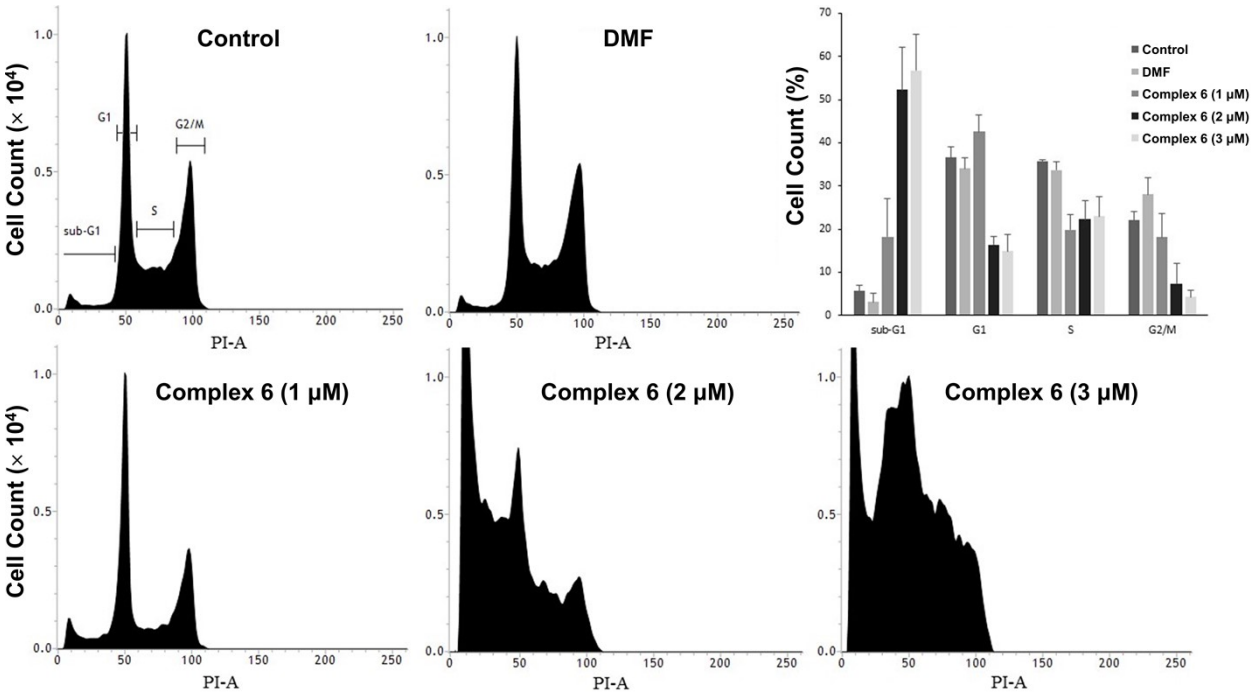

Figure S25. The cell cycle analysis in KMS12-PE myeloma cell line after 24 h treatment with 1–3 μM concentrations of **6**. Ctrl = medium, DMF = medium with DMF (the same concentration as for experiments with **6**).

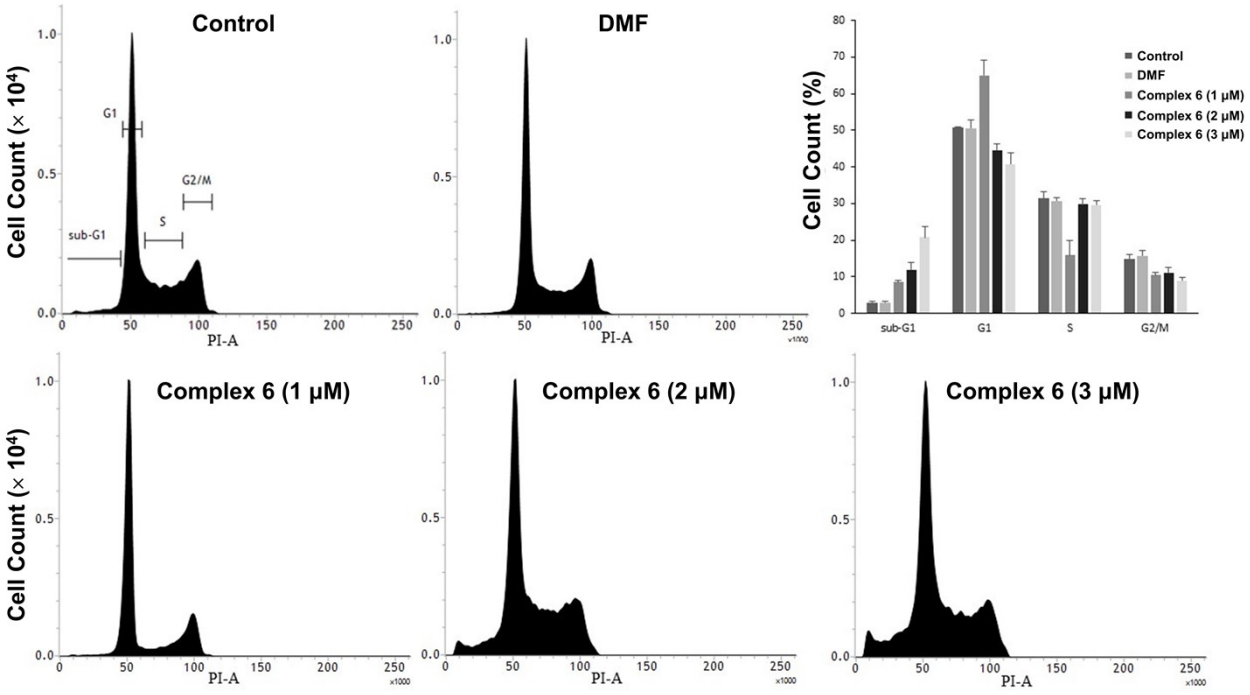

Figure S26. The cell cycle analysis in co-cultures of myeloma cell lines U266B1 with HS5 fibroblasts after 24 h treatment with 1–3 μM concentrations of **6**. Ctrl = medium, DMF = medium with DMF (the same concentration as for experiments with **6**).

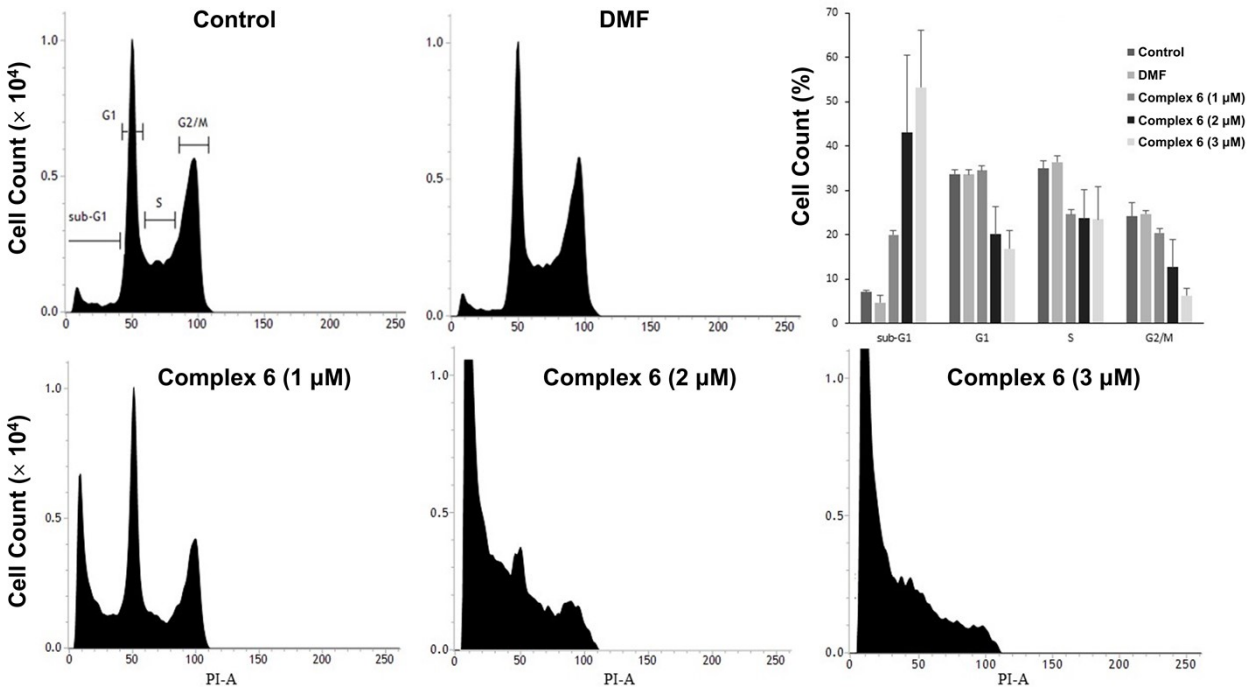

Figure S27. The cell cycle analysis in co-culture of myeloma cell line KMS12-PE and stromal fibroblast cell line HS-5 after 24 h treatment with 1μM, 2 μM, and 3 μM concentrations of complex **6**.

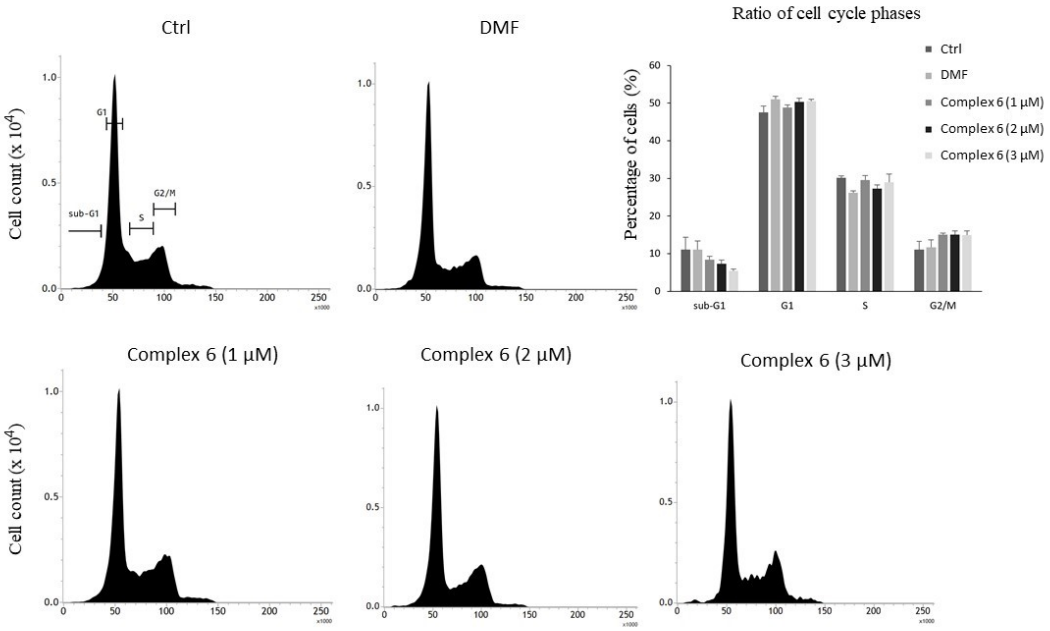

Figure S28. The cell cycle analysis of stromal fibroblast cell line HS-5 after 24 h treatment with 1 μM, 2 μM, and 3 μM concentrations of complex **6**.

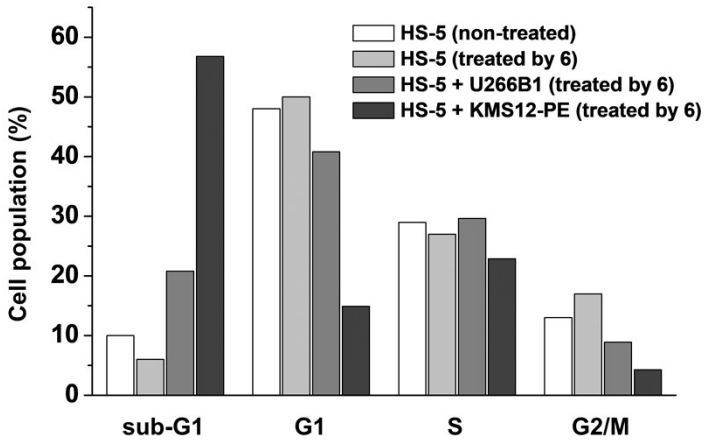

Figure S29. The cell cycle analysis in HS-5 fibroblasts and their co-cultures with U266B1 and KMS12-PE cells treated by complex **6** (non-treated HS-5 cells are given for comparative purposes).

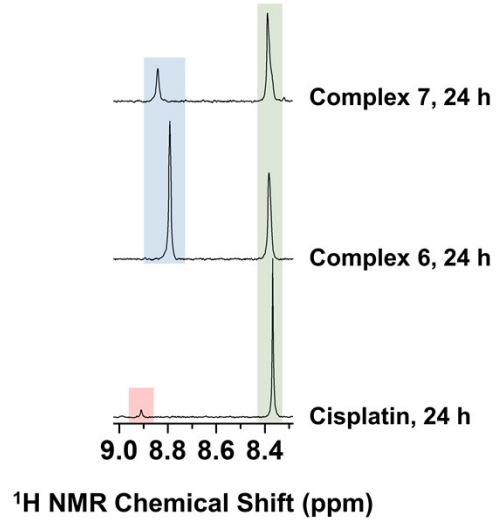

Figure S30. ^{1}H NMR studies of complexes **6** and **7** (and cisplatin for comparative purposes) in 50% DMF-d_7/50% D_2O with 2 molar equiv. of guanosine monophosphate (GMP), as observed after 24 h of standing. Blue - C2–H resonances of **6** and **7**, green - free GMP (8.37 ppm), red - cisplatin–GMP adduct (8.91 ppm).

Table S1. Crystallographic data for **3**–**5** and **7**.

	3	**4**	**5**	**7**
Chemical formula	$C_{22}H_{24}I_2N_4Pt$	$C_{18}H_{16}I_2N_4Pt$	$C_{20}H_{20}I_2N_4O_2Pt$	$C_{18}H_{16}Cl_2I_2N_4Pt$
M_r	793.349	737.241	797.294	806.130
Crystal system	Triclinic	Triclinic	Monoclinic	Orthorhombic
Space group	*P*–1	*P*–1	$P2_1/n$	*P*bca
T / K	100(1)	100(1)	100(1)	100(1)
a / Å	6.8687(1)	9.9023(2)	14.6066(2)	18.6140(2)
b / Å	11.76515(1)	10.1391(2)	10.2403(1)	20.7625(3)
c / Å	15.2867(2)	10.6636(2)	30.3372(6)	22.6035(2)
α / °	99.138(1)	67.159(1)	90	90
β / °	100.075(1)	81.854(1)	92.561(2)	90
γ / °	90.100(1)	81.997(1)	90	90
V / Å^3	1188.70(3)	972.55(3)	4533.18(12)	8735.65(18)
Z	2	2	8	16
λ / Å	0.56083	0.56083	0.56083	0.56083
Abs. correction	Multi-scan, LANA	Multi-scan, LANA	Multi-scan, LANA	Multi-scan, LANA
μ / mm^{-1}	4.552	5.557	4.778	2.414
Crystal size / mm	0.21 × 0.09 × $\hat{2}.\hat{2}\hat{1}7$	0.15 × 0.05 × $\hat{2}.\hat{5}\hat{1}8$	0.24 × 0.12 × $\hat{2}.\hat{3}\hat{3}6$	0.13 × 0.12 × $\hat{5}.\hat{0}\hat{7}2$
ρ_{calc} / g.cm^{-3}				
S	1.062	1.050	0.954	0.970
R_1 [$I > 2\sigma(I)$]	0.0110	0.0165	0.0157	0.0163
wR_2 [all data]	0.0262	0.0454	0.0363	0.0405
□□$_{max}$, □□$_{min}$ / e Å^{-3}	0.95, –0.66	1.29, –1.59	0.58, –0.52	0.44, –0.76
CCDC	2211813	2211814	2211815	2211816

Table S2. *In vitro* antiproliferative activity results for complexes **1**–**7** applied at 1–3 μM concentrations in the myeloma cell lines U266B1 and KMS12-PE, given as cell viability percentage; PE = pleural effusion due to plasma cell infiltration. Cisplatin is given for comparative purposes. Data are displayed as mean ± SD.

Compound	**U266B1**				**KMS12-PE**			
	1 μM	2 μM	3 μM	10 μM	1 μM	2 μM	3 μM	10 μM
1	95.0±1.6	83.0±8.1	73.5±3.5	N.A.	56.5±3.5	23.6±4.5	9.3±6.0	N.A.
2	93.5±4.5	83.5±4.5	57.0±13.0	N.A.	36.0±5.0	9.0±2.0	3.5±1.5	N.A.
3	85.5±1.5	35.5±6.5	6.0±2.0	N.A.	33.0±4.0	3.5±0.5	2.2±1.8	N.A.
4	83.6±8.3	44.5±11.5	8.6±4.4	N.A.	45.5±4.5	8.6±4.6	2.3±1.2	N.A.
5	72.5±7.5	20.0±7.0	4.0±1.0	N.A.	29.0±2.0	4.0±2.0	1.5±0.5	N.A.
6	64.5±0.5	9.0±2.0	3.0±1.0	N.A.	11.5±0.5	2.0±1.0	1.1±0.9	N.A.
7	11.5±3.5	3.5±1.5	2.5±1.5	N.A.	2.1±1.9	0.3±0.2	0.6±0.5	N.A.
Cisplatin	97.4±3.7	93.2±4.9	93.1±5.4	74.1±8.3	92.6±0.11	91.8±1.1	88.3±2.2	53.2±7.8

Table S3. Cell viability after the treatment with complex **6** in human solid cancer cell lines. DU-145 = prostate cancer, HepG2 = hepatocellular carcinoma, MCF-7 = breast cancer. Data are displayed as mean ± SD.

Compound	DU-145	HepG2	MCF-7
6	97±5	78±6	73±6
Cisplatin	74±3	61±4	80±3

Table S4. The populations of viable U266B1 and KMS12-PE myeloma cells (*left*) and their co-cultures with HS-5 stromal fibroblasts (*right*) after the treatment with complex **6** detected by determination of caspase 3/7 activities. Data are displayed as mean (%) ± SD (*p*-value in parentheses). The arcsin transformation was used to transform the percentage data. The significance was determined using Student's t-test for two independent means at **p* <0.05, ***p* <0.01, ****p* <0.001 (*p*-value *versus* control/solvent DMF).

	Single culture of myeloma cells				**Co-culture of myeloma and fibroblast cells**			
	U266B1				**U266B1 + HS-5**			
	DMF	**1 µM**	**2 µM**	**3 µM**	**DMF**	**1 µM**	**2 µM**	**3 µM**
Live cells	88.4±1.7	81.0±2.7	32.1±8.1	7.9±0.9	93.1±0.5	79.5±0.2	21.0±5.7	7.2±0.4
Early apoptosis	4.9±0.7	10.5±1.5	35.4±4.2	40.0±0.2	2.4±0.2	9.0±0.4	29.7±4.8	23.1±3.3
Late apoptosis / necrosis	6.6±1.0	8.5±1.2	32.5±3.9	52.1±1.1	4.5.±0.4	11.4±0.6	49.3±1.0	69.7±2.9
	KMS12-PE				**KMS12-PE + HS-5**			
Live cells	77.2±6.7	48.4±8.6	36.3±13.5	40.1±9.9	90.8±0.3	70.1±4.5	26.9±11.3	27.8±1.4
Early apoptosis	12.8±6.2	40.7±12.7	23.3±3.7	14.5±8.1	2.2±0.2	13.6±3.5	28.3±6.3	33.9±1.6
Late apoptosis / necrosis	9.8±1.0	20.9±8.3	40.2±4.7	43.3±15.6	6.9±0.3	16.1±3.1	44.7±14.1	38.1±0.4

Table S5. The populations of viable U266B1 and KMS12-PE myeloma cells (*left*) and their co-cultures with HS-5 stromal fibroblasts (*right*) after the treatment with complex **6** detected by Annexin-V staining. Data are displayed as mean (%) ± SD (*p*-value in parentheses). The arcsin transformation was used to transform the percentage data. The significance was determined using Student's t-test for two independent means at **p* <0.05, ***p* <0.01, ****p* <0.001 (*p*-value *versus* control/solvent DMF).

	Single culture of myeloma cells				**Co-culture of myeloma and fibroblast cells**			
	U266B1				**U266B1 + HS-5**			
	DMF	**1 μM**	**2 μM**	**3 μM**	**DMF**	**1 μM**	**2 μM**	**3 μM**
Live cells	78.1±1.4	72.8±1.8	41.4±22.0	6.8±2.9	80.8±3.6	64.2±2.0	20.3±3.8	9.7±1.3
Early apoptosis	10.4±1.1	14.9±0.9	40.1±5.8	49.8±2.5	8.0±2.7	17.4±1.7	41.1±5.1	44.0±7.1
Late apoptosis	10.8±2.7	11.5±3.1	26.1±6.1	42.2±1.3	9.5±2.2	16.7±1.6	36.2±2.9	43.6±6.1
	KMS12-PE				**KMS12-PE + HS-5**			
Live cells	68.2±12.6	31.1±0.1	11.6±7.3	7.6±2.8	69.5±9.7	38.9±13.2	6.9±0.5	8.5±0.9
Early apoptosis	13.2±9.3	38.8±5.3	54.1±6.5	58.0±2.8	12.5±4.3	34.6±7.6	56.1±4.2	55.1±0.1
Late apoptosis	11.1±1.4	25.6±6.1	31.1±14.6	30.9±5.1	14.2±3.7	24.4±6.0	35.6±3.5	32.3±1.4

Table S6. The cell cycle phase populations determined by flow cytometry in U266B1 and KMS12-PE myeloma cells (*left*) and their co-cultures with HS-5 stromal fibroblasts (*right*) after the treatment with 1–3 μM concentrations of **6** for 24 h. Data are displayed as mean (%) ± SD (*p*-value in parentheses). The arcsin transformation was used to transform the percentage data. The significance was determined using Student's t-test for two independent means at **p* <0.05, ***p* <0.01, ****p* <0.001 (*p*-value *versus* control/solvent DMF).

	Single culture of myeloma cells					**Co-culture of myeloma and fibroblast cells**			
	U266B1					**U266B1 + HS5**			
	sub-G_1	G_1	S	G_2/M		sub-G_1	G_1	S	G_2/M
DMF	3.0±1.2	50.6±2.4	30.7±0.4	15.7±1.9		2.7±0.4	54.1±2.1	28.0±0.8	15.2±1.5
6 (1 μM)	8.5±1.0 (0.007**)	65.0±1.5 (0.002**)	15.9±1.0 (<0.001***)	10.5±0.4 (0.021*)		3.9±0.4 (0.045*)	61.6±4.1 (0.084)	18.6±4.1 (0.032*)	15.6±0.8 (0.740)
6 (2 μM)	11.9±3.2 (0.004**)	44.6±8.9 (0.425)	29.7±8.2 (0.881)	11.1±2.9 (0.132)		12.4±2.1 (0.003**)	41.9±1.7 (0.003**)	33.4±1.6 (0.012*)	12.3±1.5 (0.121)
6 (3 μM)	20.8±2.6 (<0.001***)	40.8±9.2 (0.188)	29.6±10.6 (0.902)	8.9±1.2 (0.041*)		13.8±3.0 (0.006**)	42.0±3.0 (0.009**)	31.5±1.0 (0.012*)	12.7±0.9 (0.116)
	KMS12PE					**KMS12PE + HS5**			
DMF	3.1±0.9	34.0±2.5	33.7±1.8	28.0±4.0		4.7±1.6	33.6±1.1	36.4±1.5	24.7±0.8
6 (1 μM)	18.2±8.9 (<0.001***)	42.6±3.9 (0.018*)	19.8±3.6 (<0.001***)	18.1±5.5 (0.045*)		20.0±11.9 (0.001**)	34.5±4.6 (0.802)	24.6±5.3 (0.038*)	20.4±1.7 (0.031*)
6 (2 μM)	52.2±9.9 (<0.001***)	16.4±1.9 (<0.001***)	22.3±4.2 (0.005**)	7.4±4.6 (<0.001***)		43.1±17.4 (<0.001***)	20.1±6.2 (0.037*)	23.7±6.5 (0.039*)	12.7±6.2 (0.002**)
6 (3 μM)	56.8±8.3 (<0.001***)	14.9±3.7 (<0.001***)	22.9±4.5 (0.008**)	4.3±1.6 (<0.001***)		53.2±12.9 (<0.001***)	16.9±4.2 (0.002**)	23.5±7.4 (0.012*)	6.3±1.6 (<0.001***)

References

1. J. Koziskova, F. Hahn, J. Richter and J. Kozisek, Comparison of Different Absorption Corrections on the Model Structure of Tetrakis (μ^2-acetato)-diaquadicopper(II), *Acta Chim. Slovaca*, 2016, **9**, 136–140.
2. G. M. Sheldrick, SHELXT-Integrated Space-group and Crystal-structure Determination, *Acta Crystallogr.*, 2015, **A71**, 3–8.
3. L. Palatinus and G. Chapuis, SUPERFLIP- a Complete Program for the Solution of Crystal Structures by Charge Flipping in Arbitrary Dimensions, *J. Appl. Crystallogr.*, 2007, **40**, 786–790.
4. L. J. Bourhis, O. V. Dolomanov, R. Gildea, J. A. K. Howard and H. Puschmann, The Anatomy of a Comprehensive Constrained, Restrained Refinement Program for the Modern Computing Environment Olex2 Dissected, *Acta Crystallogr.*, 2015, **A71**, 59–75.
5. O. Dolomanov, L. J. Bourhis, R. Gildea, J. A. Howard and H. Puschmann, OLEX2: A Complete Structure Solution, Refinement and Analysis Program, *J. Appl. Crystallogr.*, 2009, **42**, 339–341.
6. F. Neese, Software Update: The ORCA Program System Version 4.0. *WIREs Comput. Mol. Sci.*, 2018, **8**, e1327.
7. P. Pollak and F. Weigend, Segmented Constrained Error-consistent Basis Sets of Double- and Triple-ζ Valence Quality for One- and Two-component Relativistic All-electron Calculations, *J. Chem. Theory Comput.*, 2017, **13**, 3696–3705.
8. D. Andrae, U. Häussermann, M. Dolg, H. Stoll and H. Preuss, Energy-adjusted *ab Initio* Pseudopotentials for the Second and Third Row Transition Elements, *Theor. Chim. Acta*, 1990, **77**, 123–141.
9. C. Adamo and V. Barone, Toward Reliable Density Functional Methods without Adjustable Parameters: The PBE0 Model, *J. Chem. Phys.*, 1999, **110**, 6158–6169.
10. F. Kleemiss, O. V. Dolomanov, M. Bodensteiner, N. Peyerimhoff, L. Midgley, L. J. Bourhis, A. Genomi, L. A. Malaspina, D. Jayalitaka, J. L. Spencer, F. White, B. Grundkötter-Stock, S. Steinhauer, D. Lentz, H. Puschmann and S. Grabowsky, Accurate Crystal Structures and Chemical Properties from NoSpherA2, *Chem. Sci.*, 2021, **12**, 1675–1692.
11. F. H. Allen and I.J. Bruno, Bond Lengths in Organic and Metal-organic Compounds Revisited: X–H Bond Lengths from Neutron Diffraction Data, *Acta Crystallogr.*, 2010, **B66**, 380–386.
12. C. F. Macrae, I. Sovago, S. J. Cottrell, P. T. A. Galek, P. McCabe, E. Pidcock, M. Platings, G. P. Shields, J. S. Stevens, M. Towler and P. A. Wood, Mercury 4.0: From Visualization to Analysis, Design and Prediction, *J. Appl. Crystallogr.*, 2020, **53**, 226–235.